Space Sci Rev
DOI 10.1007/s11214-009-9557-y

Crustal Magnetic Fields of Terrestrial Planets

Benoit Langlais · Vincent Lesur · Michael E. Purucker · Jack E. P. Connerney · Mioara Mandea

Received: 2 March 2009 / Accepted: 15 June 2009

Abstract Magnetic field measurements are very valuable, as they provide constraints on the interior of the telluric planets and Moon. The Earth possesses a planetary scale magnetic field, generated in the conductive and convective outer core. This global magnetic field is superimposed on the magnetic field generated by the rocks of the crust, of induced (i.e. aligned on the current main field) or remanent (i.e. aligned on the past magnetic field). The crustal magnetic field on the Earth is very small scale, reflecting the processes (internal or external) that shaped the Earth. At spacecraft altitude, it reaches an amplitude of about 20 nT. Mars, on the contrary, lacks today a magnetic field of core origin. Instead, there is only a remanent magnetic field, which is one to two orders of magnitude larger than the terrestrial one at spacecraft altitude. The heterogeneous distribution of the Martian magnetic anomalies reflects the processes that built the Martian crust, dominated by igneous and cratering processes. These latter processes seem to be the driving ones in building the lunar magnetic field. As Mars, the Moon has no core-generated magnetic field. Crustal magnetic features are very weak, reaching only 30 nT at 30-km altitude. Their distribution is heterogeneous too, but the most intense anomalies are located at the antipodes of the largest impact basins.

B. Langlais
Laboratoire de Planétologie et Géodynamique, CNRS UMR 6112, 2 rue de la Houssinière, 44000 Nantes, France

B. Langlais (✉)
Laboratoire de Planétologie et Géodynamique, Université de Nantes, 2 rue de la Houssinière, 44000 Nantes, France
e-mail: benoit.langlais@univ-nantes.fr

V. Lesur · M. Mandea
Helmholtz Centre Potsdam, German Research Centre for Geosciences, Potsdam, Germany

M.E. Purucker
Raytheon at Planetary Geodynamics Laboratory, Code 698, NASA Goddard Space Flight Center, Greenbelt, MD 20771, USA

J.E.P. Connerney
Planetary Magnetospheres Laboratory, Code 695, NASA Goddard Space Flight Center, Greenbelt, MD 20771, USA

Published online: 03 July 2009

The picture is completed with Mercury, which seems to possess an Earth-like, global magnetic field, which however is weaker than expected. Magnetic exploration of Mercury is underway, and will possibly allow the Hermean crustal field to be characterized. This paper presents recent advances in our understanding and interpretation of the crustal magnetic field of the telluric planets and Moon.

Keywords Magnetic Field · Telluric Planets · Crust · Measurements · Modeling Techniques · Interpretation

1 Introduction

The description and the understanding of the magnetism associated with rocks has always been a very important topic, for both fundamental and applied sciences. The Chinese were probably the first to use compasses for orientation purposes (Needham 1962), with a south-pointing iron needle, or "Si Nan". The use of the compass for marine navigation was introduced in Europe during the 12th century, even if the reason why it was indicating the North pole (or the South one) was not well understood. For some, compasses were showing the polar star, and for others it was indicating the location of a close-to-the-pole island, where magnetite was mined. The first scientific explanation came in 1600, when William Gilbert published the results of his experiments with a spherical magnets called "terrelae" (Gilbert 1600). Among other conclusions, he proposed that the magnetic field of the Earth was not stationary, but that instead it was rotating together with the Earth. He also correctly assumed that the center of the Earth was made of iron. However, as shown in Fig. 1, he erroneously attributed the deviation of the compass to the presence of positive or negative imperfections on the sphere, such as oceanic areas or land masses.

William Gilbert was not completely wrong. Land masses may indeed deviate the compass needle from the pure intern geomagnetic pole. Rocks of the upper lithosphere (or crust) of

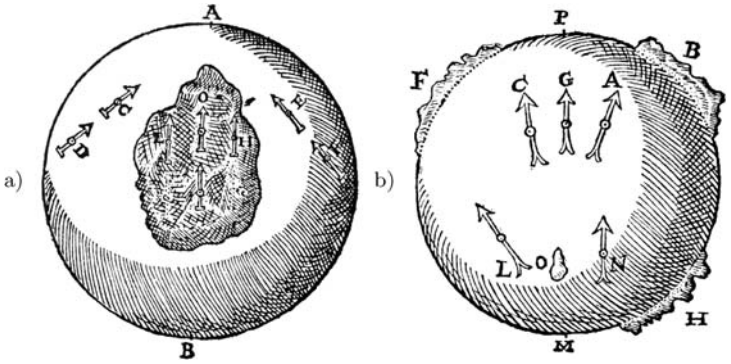

Fig. 1 Behavior of the magnetic compass or vector as a function of land masses, as imagined by Gilbert (1600). (**a**) A and B denote North and South poles, respectively. Compasses C, D, E and F show the true magnetic pole, because they are distant from the "imperfect and weaker" part (the imperfect part is meant to resemble an oceanic area). Compass O also shows the pole, as it is located in the middle of the imperfection. On the contrary, H and L compasses deviate towards the edges of the imperfect area. (**b**) P and M denote North and South poles, respectively. Imperfections in B, F, H, and O are positive anomalies, or land masses. Compass G shows the pole, as it is equidistant from F and B. On the contrary, A and C compasses deviate toward B and F, respectively. Compass L shows pole M, as O is too small to affect it. But compass N is deviated by H

the Earth and other planets such as the Moon and Mars may produce a magnetic field, whether it is induced by an internal or external source, or remanent. Actually, everything is magnetic, from a piece of wood to a plate of steel. This effect, known as diamagnetism, is a result of the interaction of orbiting electrons within an external magnetic field. This produces an opposite direction magnetic field of relatively small magnitude. More important is the paramagnetism effect. It affects only atoms which possess an atomic magnetic moment. The induced magnetization is aligned and parallel to the applied magnetic field, but it will return to zero if the applied magnetic field is removed. This effect is inversely proportional to temperature. The most important effect is ferromagnetism: this also affects atoms with magnetic moment, but in this case, adjacent atomic magnetic moments strongly interact, allowing the material to retain a magnetic field even in the absence of an external magnetic field.

Ferromagnetic materials are mainly iron, cobalt and nickel. Of these, iron is by far the most common in nature. Combined with oxygen, iron is found as hematite and magnetite in common rock types. Titanium often replaces some of the iron in both the more oxidized hematite, and the less oxidized magnetite. These Fe–Ti oxides are also common magnetic phases in many rock types. Some iron sulfides (e.g. pyrrhotite) and oxyhydroxides (e.g. goethite) are also common magnetic phases in rocks (Weiss et al. 2009). Such minerals are capable of bearing both remanent and induced magnetization. The Koenigsberger ratio measures the relative importance of the induced M_i to the remanent M_r contribution. To first order, induced magnetization is parallel and proportional to the direction and intensity of the external field $\mathbf{B}$. The proportionality is expressed through χ, the magnetic susceptibility, which mainly depends on the magnetic mineralogy. The relation between the remanent and the original (i.e. the one that gave the minerals their remanence) is less simple. It depends on several factors, among which is the Curie temperature. This is the temperature above which magnetic minerals loose their remanent magnetization. The Curie temperature of magnetite and hematite, the most commonly found terrestrial magnetic minerals, is 580°C and 670°C, respectively. For titanomagnetites and titanohematites, the Curie temperature decreases as the Ti content increases. Other important parameters are the magnetic mineralogy, the grain size and shape. The M_r versus $\mathbf{B}$ behavior can be described by an hysteresis loop (see Dunlop and Özdemir 1997 for a review).

The Earth and Mars are very alike in the sense that they are basically made of similar components. Together with Venus and Mercury, they constitute the telluric planets, with are primarily composed of silicate rocks. These planets are differentiated, with a core, a mantle and a crust. For simplicity, we include the Moon in that category too, although the existence of a Lunar core is debated (Lognonné et al. 2003).

On the Earth, the main present-day magnetic field has a deep origin. It originates from the outer liquid core, where convection of a conducting fluid create a (mostly) dipolar, axial and centered magnetic field. At the Earth's surface, this main field ranges from about 20,000 nT at the magnetic equator to 70,000 nT at the magnetic poles. It is time variable, on different time scales. The most dramatic variations correspond to the inversion of the polarity of the field. Such inversions are recorded by magnetic minerals when they cool down below their Curie temperature. Intensity variation (or secular variation) exists too and may also be recorded by minerals. Shorter terms variations are most of the time related to external sources. The magnetic field of the crust is often referred as the anomaly field. These anomalies are actually fields in excess or in deficit of the main field. Terrestrial magnetic anomalies are therefore positive or negative, while they are only positive for Mars and the Moon, where there is no core field. Fields of crustal origin can be very intense, up to 200,000 nT near Kursk (Jankowski and Sucksdorff 1996), but they decrease very fast as the distance

to the source increase. At 400 km altitude, crustal fields are estimated to range between ±20 nT (Mandea and Purucker 2005). In the following, the words crust and lithosphere are often used interchangeably. 'Crust' is differentiated from 'mantle' on the basis of its chemical composition, while 'lithosphere' is a rheological term and usually comprises the strong crust and uppermost mantle. Magnetic rocks are confined to regions of the crust and upper mantle cooler than the Curie temperature, defining a magnetic crust or lithosphere. Most upper mantle rocks are non-magnetic, even if they are cooler than the Curie temperature, because iron is overwhelmingly in silicates, not in oxides. Serpentinite with magnetite is an exception to this rule, and can be found in the mantle overlying subduction zones.

In this review paper, we first introduce the modeling and representing techniques, on both global and local scales, with associated limits and caution. We then summarize magnetic measurements and maps that were acquired around the Earth, Mars, Mercury, Venus and the Moon. We will focus only on the magnetic field of crustal and lithospheric origin; those interested in the core magnetic field and in the external magnetic field are referred to Hulot et al. (2009) and to Baumjohann et al. (2009). We finally review recent developments and interpretations of magnetic measurements in terms of planetary dynamics or surface processes, and conclude with open issues and perspectives.

2 Modeling Techniques and Issues

The acquisition of magnetic measurements above the surface of a planet is challenging, but the interpretation of these measurements in terms of magnetic field model or magnetization distribution is also difficult. In the following, we briefly review the modeling techniques used. We make the distinction between techniques used to describe the field and those used to interpret the field in terms of source properties.

2.1 Modeling the Field

The magnetic field is measured on a discrete basis, along the spacecraft trajectory, in the air, or on the ground. It is of course possible to average measurements onto regular grids, but a more powerful technique consists in building a continuous description of the field on the surface of a sphere. This is commonly done with spherical harmonics, but other methods exist.

Spherical Harmonics (SH) form the natural basis to describe a potential field on a spherical surface because they are the eigen functions of the Laplacian in spherical geometry. As such, they form the smallest set of functions that can describe all possible potential fields up to a given wavelength. Furthermore, if a magnetic field is described in terms of spherical harmonics, the separation of the field due to sources internal to the observation (internal dynamo or magnetized rocks), from those due to external sources (magnetospheric field) can in theory be performed. In geo- and planetary magnetism, the Schmidt semi-normalized spherical harmonics are commonly used.

Away from the magnetic sources, the magnetic field is therefore described as the gradient of a potential, following $\mathbf{B} = -\nabla V(\theta, \phi, r, t)$. The potential is a function of colatitude θ, longitude ϕ, radius r and time t. An internal and an external potential are associated with this poloidal field, V_i and V_e respectively. They are described on a spherical surface by:

$$V_i(\theta, \phi, r, t) = a \sum_{n=1}^{N_i} \sum_{m=0}^{n} \left(\frac{a}{r}\right)^{n+1} \left(g_n^m(t) \cos(m\phi) + h_n^m(t) \sin(m\phi)\right) P_n^m(\cos\theta) \quad (1)$$

$$V_e(\theta,\phi,r,t) = a\sum_{n=1}^{N_e}\sum_{m=0}^{n}\left(\frac{r}{a}\right)^n \left(q_n^m(t)\cos(m\phi) + s_n^m(t)\sin(m\phi)\right) P_n^m(\cos\theta), \quad (2)$$

where a is the reference radius, $P_n^m(\cos\theta)$ are the Schmidt quasi-normalized associated Legendre functions of degree and order n and m, and $(g_n^m(t), h_n^m(t))$, $(q_n^m(t), s_n^m(t))$ are the Gauss internal and external coefficients, respectively. As the upper bound N_i and N_e of these summations increase, the magnetic field is described, globally, in more details, i.e. with shorter wavelengths. For a given value of N_i the number of Gauss coefficients describing the internal field is $N_i(N_i+2)$.

The drawbacks in describing the field in terms of spherical harmonics comes from the global nature of these functions. A data set rarely covers the whole planet, e.g. for satellite data a hole generally remains close to the poles, and therefore the spherical harmonic model is prone to oscillations. Furthermore, over a planet the spectral content of the observed magnetic field may vary, and therefore the required resolution of the model may not be the same everywhere. Typically for the Earth, at satellite altitudes, the oceanic crust is nearly free of sharp and strong anomalies and does not need high degree spherical harmonics, whereas over continental areas very small details are present and require a sharper description. Constraining locally the spherical harmonic model is possible (Lesur 2006) but this has been infrequently used.

Wavelets or localized basis are an interesting alternative to SH. This representation technique replaces the usual global spherical harmonic expansion of the potential by a summation over functions of the type:

$$\mathcal{F}_i(\theta,\phi) = \sum_{n,m}^{N} f_n\, Y_n^m(\theta_i,\phi_i) Y_n^m(\theta,\phi). \quad (3)$$

In this expression, (θ_i, ϕ_i) is the center of the function. The upper bound to the summation, N, can tend to infinity if required, and the f_n are adjusted to "concentrate" the function in both spatial and spectral domains. These techniques have been infrequently used for modeling the crustal field even if they allow for a varying resolution over the sphere. They can also be used for building localized models. Localized functions have been applied by Lesur and Maus (2006). One can refer to the work of Chambodut et al. (2005) for wavelets. Also, vector scaling wavelets have been used for modeling the Earth's crust (Mayer and Maier 2006).

Spherical Cap Harmonics Analysis (SCHA) is possibly the most frequently used method on the sphere that uses local basis functions. It was developed by Haines (1985) to model the main magnetic field over small areas and has, since then, been applied in a large variety of circumstances (see Torta et al. 2006 for a review). As for SH, the internal potential is expressed as a sum:

$$V_i(\theta,\phi,r,t) = a\sum_{k\geq m}\sum_{m\geq 0}\left(\frac{a}{r}\right)^{n_k+1} \left(G_{n_k}^m(t)\cos(m\phi) + H_{n_k}^m(t)\sin(m\phi)\right) P_{n_k}^m(\cos\theta). \quad (4)$$

In this expression, the order m is integer, and the degree n_k is generally real, with $n_k \geq m$. SCHA has some fundamental limitations, in particular with respect to the separation of internal from external fields. Also of concern is the assimilation of multi-level data (Thébault

and Gaya-Piqué 2008). A revised SCHA was proposed recently (Thébault et al. 2006a), addressing the problem of altitude and multi-level data compatibility. This was used to merge ground and satellite data (Thébault et al. 2006b). A specific formalism was recently developed to process ground data only (Thébault 2008).

Equivalent Source Dipole (ESD) is the alternate and often used technique for global description of magnetic field around planets. This method was introduced by Mayhew (1979). Considering the magnetic moment $\mathbf{M}$ of a given dipole located at (r_d, θ_d, ϕ_d), the magnetic potential observed at (r, θ, ϕ) is expressed as

$$V_i = -\mathbf{M} \cdot \nabla \frac{1}{l}. \tag{5}$$

This relation is valid provided that there are no sources between the dipole and the observation location. The distance l between the dipole and the observation location is written:

$$l = \left(r_d^2 + r^2 - 2r_d r \left[\cos(\theta)\cos(\theta_d) + \sin(\theta)\sin(\theta_d)\cos(\phi - \phi_d)\right]\right)^{\frac{1}{2}}. \tag{6}$$

The observed magnetic field $\mathbf{B}$ is the gradient of the potential V_i due to a series of dipole sources located inside the planet. This method was primarily designed to reduce scattered measurements to a common altitude.

This method has several advantages. First, it associates with a magnetic data set, information about the magnetization distribution. If carefully used, this information can be useful but a simplistic direct interpretation may lead to erroneous conclusions as described below. Second, as for the localized methods, the resolution in both spatial and spectral domain can be changed by modifying the density of the dipoles or their depths. This freedom carries also difficulties because, for a given source depth, the density has to be high enough in order to avoid spurious model magnetic field behavior. As a result, the number of required dipoles is usually relatively high. For a given resolution (i.e. a given maximum spherical harmonic degree), the number of parameters is as least twice as large as the number of requested Gauss' coefficients. When used to model terrestrial magnetic field anomalies, one can use *a priori* information to constrain the model (and to reduce the number of parameters). For instance a purely induced magnetization aligned onto the core field is often assumed over the continents (Purucker et al. 1998).

2.2 Modeling the Magnetization

We now turn to the methods for extracting the magnetization information from the data. The magnetic field $\mathbf{B}$ is linked to the rock magnetization by the relation:

$$\mathbf{B}(\mathbf{r}) = \int_v \mathbf{G}(\mathbf{r}, \mathbf{s}) \cdot \mathbf{M}(\mathbf{s}) dv. \tag{7}$$

where $\mathbf{r}$ and $\mathbf{s}$ are two points in space, outside and inside the magnetized volume v respectively. $\mathbf{G}(\mathbf{r}, \mathbf{s})$ is the usual Green tensor given by:

$$\mathbf{G}(\mathbf{r}, \mathbf{s}) = -\frac{\mu_0}{4\pi} \nabla_{\mathbf{r}} \nabla_{\mathbf{s}} \frac{1}{|\mathbf{r} - \mathbf{s}|} \tag{8}$$

The most often used techniques consist in describing the magnetization in term of spherical uniformly magnetized bodies (i.e. dipoles), sometimes uniformly magnetized cylinders for

2-D geometry, or as a discrete sum of the Green tensors themselves (Parker et al. 1987). Other techniques are described in Blakely (1995), Purucker and Whaler (2007).

It is clear that the inverse problem of finding a distribution of magnetization that exactly explains the measured magnetic field suffers from fundamental non-uniqueness. There indeed exist magnetization distributions, also known as magnetic annihilators, which do not produce significant magnetic field outside of the magnetized area (Runcorn 1975; Lesur and Jackson 2000). As a simple example given by Parker et al. (1987), if f is an arbitrary continuously differentiable function, the magnetization $\mathbf{M} = \nabla f$ defined in a volume v does not produced any external field when the function f vanishes on the boundary of the magnetized volume. This is a simple implication of the Gauss' theorem. Even if very strong constraints are applied on the magnetization distribution, as in the dipole representation, the magnetization distribution is not unique: a sufficient number of radially magnetized dipoles can always explain a finite set of vector magnetic measurements (Purucker et al. 2000).

A possible way for deriving information about the magnetization is to search for minimum norm solutions. Instead of looking for the best fit to the data without imposing any constraints on the solution, the continuously varying magnetization is bounded so that its rms amplitude is minimal (Whaler and Langel 1996). For the Earth's case the hypothesis of purely induced magnetization is often used. This is generally a sufficient hypothesis to resolve the non-uniqueness of the magnetization, although on global scale the inverse problem still present difficulties (Maus and Haak 2003). On more local scale, it is possible to resolve the non uniqueness by imposing strict source geometries, such as disks, cylinders or spheres (Quesnel et al. 2008). In this case, a unique magnetization solution can be found to explain magnetic field measurements. However, it must be kept in mind that the magnetization estimates actually depends on the *a priori* imposed source geometry and location.

3 Magnetic Measurements and Global Maps

Magnetic measurements made around the Earth, Mars, Venus, Mercury and the Moon are described in the following. For the Earth, only the lithospheric part is discussed.

3.1 The Earth

Relative to other planets, the amount of data available for studying the Earth's lithospheric field is very large. For these studies three types of data are available, namely: aeromagnetic data, marine data and survey satellite data. The quality of the measurements depends of course on the experiment itself, but also on the capacity to remove transient variations of external origin (i.e. contributions of the ionospheric and magnetospheric current systems). This is typically done by monitoring these variations at a nearby magnetic observatory.

Airborne magnetic surveys have been commonly used for mapping the crustal magnetic field in view of mineral exploration or for studying regional crustal structures. However, because of the cost involved and other technical difficulties, these surveys are of limited extent and the information for wavelength larger than 200 km are seldom reliable. They nonetheless offer accurate mapping of the magnetic field and, since the 1950's, the accumulated set of local surveys have allowed a significant part of the northern hemisphere continental area to be covered. Australia is also fully covered and long-range surveys have been organized there to preserve the long wavelength information. However, over most of Africa and South-America, very little data is freely available. Similarly, Antarctica is only partially covered.

Over the oceanic area, away from the coast, there is little aeromagnetic survey data but marine data can be used. The processing of such survey is rather difficult because there is usually no nearby monitoring of the external field variations. Furthermore, outside small areas where specific surveys have been undertaken, the ship tracks do not form a dense and regular set of data. The interpolation process is then difficult (Dyment et al. 1995) and the accuracy of the obtained maps may be sometimes debatable. As for aeromagnetic data, the Northern Hemisphere is much better covered by marine data than the Southern Pacific, Atlantic and Indian Oceans.

Because of these uncovered areas, geomagnetic measurements on board artificial satellites were soon envisaged. The first magnetometer flew on Sputnik 3, between May 1958 and April 1960 (Dolginov et al. 1961). Satellites of the Polar Orbiting Geophysical Observatories (POGO) series were launched during the late 1960's. They carried out only scalar measurements (Langel 1990), but they provided the first maps of the crustal anomalies at mid latitudes (Regan et al. 1975). These results motivated the MAGSAT satellite mission (November 1979 to April 1980) which measured the vector component of the magnetic field. The first global SH description of the magnetic field of crustal origin was that of Cain et al. (1984). Their model is based on MAGSAT vector measurements, and described the field up to degree 29. In the following twenty years, the only satellite data available were obtained for the POGs satellite (1990–1993) launched by the US Navy, although only scalar data were returned. In February 1999 the Ørsted satellite was launched carrying both vector and scalar magnetometers (Olsen et al. 2000). Its high altitude (between 643 km and 881 km after launch) however precludes an accurate mapping of the crustal field beyond degree 30. During 2000 two satellites carrying magnetometers were launched, the CHAMP German satellite at an altitude of 450 km (Reigber et al. 2002) and the SAC-C satellite at a higher altitude (Colomb et al. 2004). The advantage of the CHAMP satellite is twofold: the satellite has acquired high quality vector data, and its low-orbit is optimized for crustal studies. In 2009, CHAMP is flying at a lower altitude of about 330 km, which, combined with the solar minimum activity, will make it possible to increase the resolution of the crustal field description.

If the quality of these modern satellites is such that the core and crustal fields can be accurately mapped, the crustal anomaly field with wavelength longer than 2500 km (i.e. SH degree < 16) remains unknown because the main core field is much stronger than the crustal field and overlaps it at these length scales: their respective contributions cannot be separated from magnetic data alone. Several models of the crustal field have been produced. The latest and best models of the crustal field have been derived from the CHAMP satellite data set.

The main difficulty when dealing with satellite magnetic data arises from the contribution of the magnetic fields generated in the magnetosphere, ionosphere and by Field Aligned Currents. Of particular concern is the part generated in the ionosphere that is seen as an internal source by satellites. To circumvent these problems one approach is to process (sometimes referred to as filtering) the survey data and to remove, as much as possible, these undesirable contributions. This is the approach used for the `MF` series of crustal magnetic field models. The first of these very successful models was the `MF1`, released on 2002 (Maus et al. 2002). It goes up to SH degree 80, and is based on CHAMP scalar magnetic data. The `MF2` came one year later and included vector satellite data. It was soon followed by the `MF3` and `MF4` versions, but none of these models have an acceptable behavior everywhere at the Earth's surface. The `MF4x` (Lesur and Maus 2006) model was built from exactly the same data set as the `MF4`, but the system of representation used localized functions which allow a varying resolution of the model depending on location. This new way of regularizing the model led to a model with an acceptable behavior at ground level. It goes up to SH degree 60 at high

latitudes and degree 90 at mid and low latitudes. In 2007 and 2008 were released the latest versions of the MF series models, the versions MF5 (Maus et al. 2007) and MF6 (Maus et al. 2008) respectively. This last model provides a SH representation of the crustal field up to a maximum degree 120 but is regularized from degree 80 onwards. The data used are scalar and vector CHAMP measurement from 2003 up to mid 2007.

An alternate method to model the crustal field can be described as the "comprehensive" approach. It consists in modeling as accurately as possible all the main sources of the magnetic field (Sabaka et al. 2004). Even though this approach has been very efficient in providing accurate models of the core magnetic field, it has been less successful regarding the crustal field. Nonetheless, the two latest of these models, GRIMM (Lesur et al. 2008) and xCHAOS (Olsen and Mandea 2008), present a remarkable agreement up to SH degree 45 (Lesur et al. 2008).

At spacecraft altitude, the magnetic field anomalies are relatively smoothed (see Fig. 2). The model of Lesur et al. (2008) predicts a field ranging between $\pm$ 20 nT. The largest fields are mostly found above the continental cratons. The most noticeable anomalies are those of Bangui (Central Africa) and Kursk (Ukraine).

One of the most important achievements in describing the Earth's crustal field was the publication of the World Digital Magnetic Anomaly Map (WDMAM) (Korhonen et al. 2007). The project was the realization of an international scientific joint effort—supported by the International Association of Geomagnetism and Aeronomy (IAGA), as well as by the Commission for the Geological Map of the World (CGMW)—to compile and publish a reliable world map of magnetic anomalies that are attributable to the Earth's uppermost lithosphere. This map is derived from a multitude of aeromagnetic surveys acquired over continents or from ship cruises, during the past five decades. For the first time, these data are referenced to satellite magnetic measurements and geomagnetic observatories in a comprehensive way. The resulting product is a printed magnetic anomaly map of the World at scale 1:50,000,000 (uniform with Geological Map of the World by CGMW) and a digital database that includes anomaly values on a grid of resolution 3 arc minutes (about 5 km at the equator). The nominal observation altitude is defined as 5 km above the geoid.

3.2 Mars

The exploration of planet Mars began in 1960 with the launch of two Soviet probes (Marsnik 1 and Marsnik 2) that failed shortly after launch (Perminov 1999). The first successful mission to Mars was the USA's Mariner 4 spacecraft, in 1965. It approached Mars within 4 radii of the planet, but did not detect anything but a bow shock (Smith et al. 1965).

Despite numerous opportunities over the next 32 years, no space probe instrumented to measure magnetic fields flew close enough to the planet's surface to establish the presence of an intrinsic magnetic field. Estimates of a Mars' magnetic dipole ranged from 0.8 to 2.55 10^{22} G $\cdot$ cm^3, equivalent to an equatorial surface field of 20 to 65 nT, but its nature and origin was highly debated (Ness 1979). The USSR's Phobos 2 mission provided observations as close as 800 km altitude. No conclusive evidence for a magnetic field of internal origin emerged (Riedler et al. 1989), but some argued in favor of a small planetary field (Dolginov and Zhuzgov 1991; Slavin et al. 1991; Moehlmann et al. 1991) or localized magnetic anomalies (Moehlmann 1992). The controversy did not end until Mars Global Surveyor (MGS) entered Mars orbit in September 1997.

MGS was instrumented with a magnetometer and electron reflectometer experiment. Two triaxial fluxgate magnetometers were mounted at the outer extremity of the solar array panels, and an electron reflectometer was mounted on the spacecraft body. The vector magne-

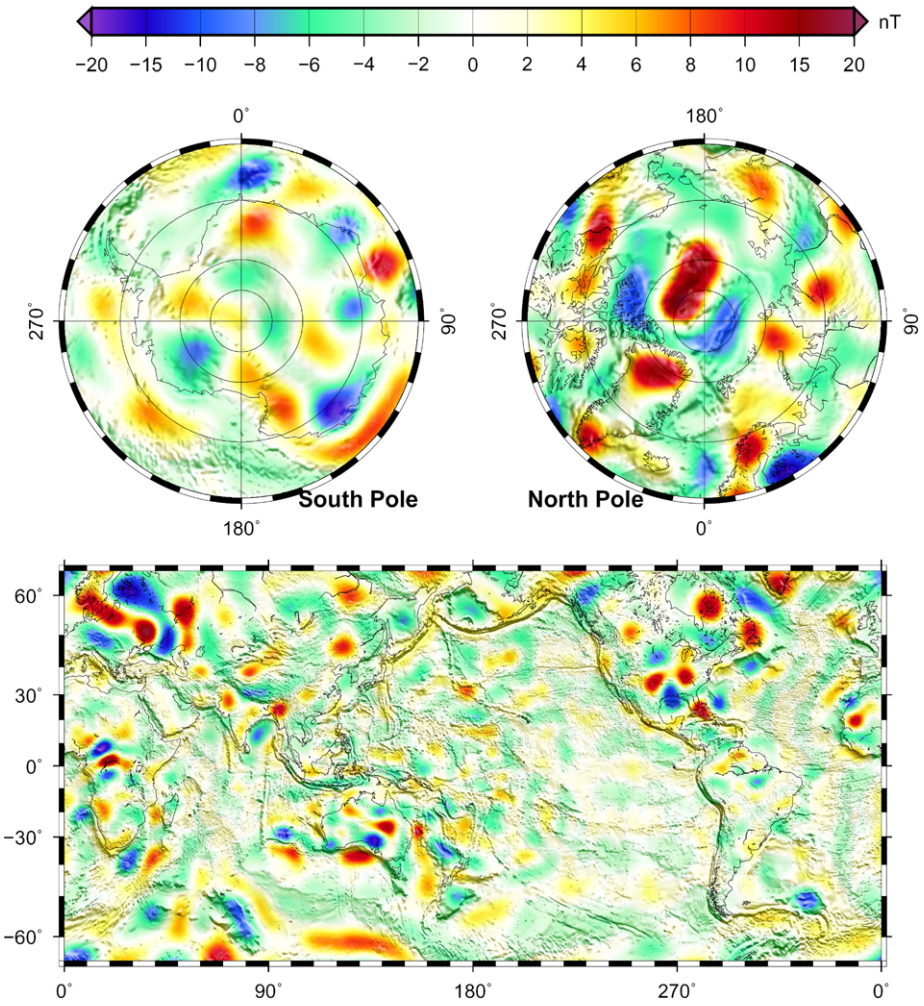

Fig. 2 Predicted radial component of the terrestrial crustal magnetic field at an altitude of 350 km above the reference radius, based on the SH model of Lesur et al. (2008) up to degree 45, superposed onto a terrestrial shaded relief (ETOPO5 1988). *Top*: South and North pole (orthographic projection), down to 60°S latitude. *Bottom*: Mercator projection between ±65°S latitude. Coastlines are plotted for clarity

tometers provided in situ measurement of the ambient magnetic field with 12-bits resolution over 8 automatically-selected dynamic ranges from ±4 nT to ±65,536 nT full scale. The electron reflectometer measured the local electron distribution function in the range of ∼10 eV to 20 keV. These measurements can be used to remotely sense the magnetic field magnitude down to altitudes of approximately 170 km, where atmospheric absorption of electrons limits the application of the electron reflection method (Mitchell et al. 2001). A detailed description of the instrumentation is found in (Acuña et al. 1992), and a discussion of the MGS spacecraft, spacecraft magnetic field mitigation, and early results are given in (Acuña et al. 2001; Connerney et al. 2004).

The MGS mission was designed to recover a subset of the science objectives of the Mars Observer mission, which ended prematurely in August, 1993, with an unsuccessful orbit

insertion maneuver. To save fuel, MGS was supposed to reach its high inclination, circular mapping orbit at 400 km altitude by aerobraking in the Mars atmosphere. This approach uses atmospheric drag to reduce apoapsis; over time, and with each periapsis pass, the elliptical orbit becomes more and more circular. As a result of a spacecraft anomaly experienced early in the mission, MGS used many more drag passes than originally intended to slow the spacecraft (Albee et al. 2001). This unanticipated development allowed a far greater than expected sampling of the magnetic field well below the nominal 400 km mapping phase altitude.

MGS observations are best described by reference to three distinct mission modes. These are the aerobraking orbits (AB), science phasing orbits (SPO), and mapping orbits (MO). The two aerobraking phases (AB1 and AB2) occurred with the spacecraft in elliptical orbit about Mars. These two phases were separated by SPO1 and SPO2, during which the spacecraft was "parked" at a fixed periapsis altitude. These four mission phases, extending through March, 1999, provided in situ observations extending down to altitudes of as little as 100 km at periapsis. During almost all AB and SPO passes, MGS acquired measurements of the vector magnetic field and electron distributions along the orbit at varying altitude above the surface. The latitude of periapsis at the beginning of AB1 was about 30°N. Subsequent orbits evolved such that the latitude at periapsis progressed slowly northward toward and over the pole through SPO2. During AB2, the latitude of periapsis progressed southward, reaching a maximum of 87°S at the end of aerobraking. At that time, 1023 aerobraking passes (subset for which magnetic field data were obtained) were distributed more or less randomly in longitude, completed by 60 (out of 130) passes for SPO1 and 211 (out of 244) passes for SPO2. By the end of pre-mapping about half of Mars' surface had been sparsely sampled at low altitude (Acuña et al. 1999).

MO observations began in March, 1999 and continued until November 2, 2006, at which time the spacecraft was lost after a series of errors that left its battery depleted, and the spacecraft unable to maintain attitude. The primary (one full Mars year, until the end of January, 2001) and the extended phases over 3 Mars years provided abundantly oversampled coverage of the magnetic field at a nominal altitude of 400 km (370–438 km) and fixed (2 am–2 pm) local time. During the mission, MGS completed 100 mapping cycles before it was lost. Each cycle lasted 28 days, providing coverage of the entire planet by using a 7-day, 88-orbit repeat geometry.

At the 400 km nominal mapping altitude, magnetic fields generated by the interaction of Mars' atmosphere with the solar wind can at times be appreciable. To first approximation, external fields draped over a conducting obstacle will align with the conducting surface (ionosphere), appearing largely in the horizontal component of the field. External fields are time variable, reflecting variations in the solar wind, and greater in magnitude near the sub-solar point. The external field is both quieter and weaker in magnitude over the darkened hemisphere (Vennerstrom et al. 2003).

The MGS vector magnetic field observations from all phases were compiled into different maps and models of the three components of the martian magnetic field. At an altitude of 400 km (see Fig. 3), the martian magnetic field varies between $\pm$ 250 nT. The largest magnetic fields are located in the Southern Hemisphere. A map at nominal mapping altitude around 400 km was produced (Connerney et al. 2001), based on night side observations only. Measurements were sorted onto 1° latitude-longitude bins, keeping only the median value to minimize transient variations. An improved map was published later (Connerney et al. 2005), using more data and a more elaborate technique for removal of external fields. However, these maps did not incorporate the early measurements of the AB and SPO low altitude phases. The first model based on those measurements was produced by Purucker

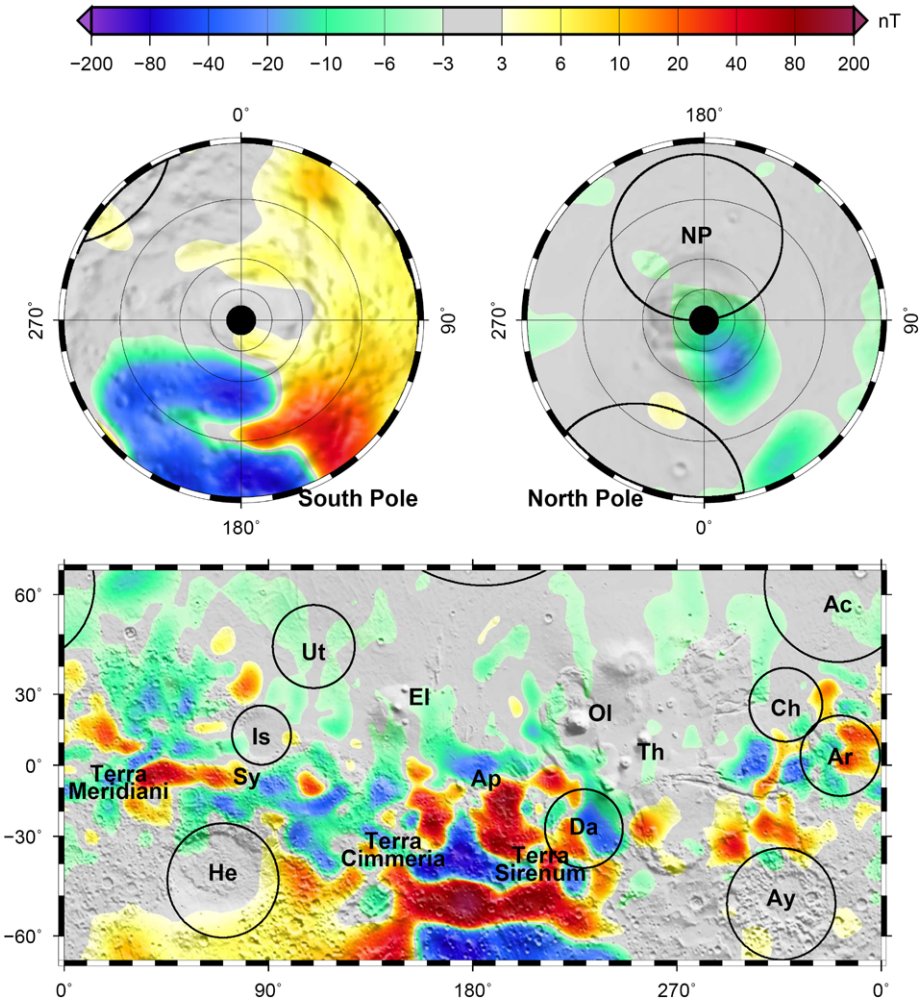

Fig. 3 Predicted radial component of the martian magnetic field at an altitude of 400 km above the martian mean radius, based on the equivalent source dipole model of Langlais et al. (2004), overlapped onto a martian shaded relief (Smith et al. 2003). *Top*: South and North pole (orthographic projection), down to 60°S latitude. *Bottom*: Mercator projection between ±65°S latitude. The main rims of the largest impact basins are plotted, with labels: He Hellas, Ar Ares, Ac Acidalia, Da Daedalia, Ay Argyre, Ch Chryse, NP North Pole, Is Isidis, and Ut Utopia. Also shown is the location of major volcanoes Sy Syrtis Major, Th Tharsis Montes, Ol Olympus Mons, El Elysium Mons, and Ap Apollinaris Patera

et al. (2000), based on binned measurements of the radial field only and an ESD approach. The first SH model (up to degree 50) of the martian magnetic field was based on the three measured components of the MO phases (Arkani-Hamed 2001a). Later models were more elaborate, and used measurements of all three mission phases, to produce SH models up to degree 90 (Cain et al. 2003; Arkani-Hamed 2004), and constant altitude maps through ESD (Langlais et al. 2004) or continuous magnetization solutions (Whaler and Purucker 2005). The MGS electron reflectometer observations have also been compiled to produce maps of the magnetic field magnitude at a reference altitude of about 170 km (Mitchell et al. 2007;

Lillis et al. 2008b) although with a somewhat lower spatial resolution. Data were also used to built local models over localized magnetic anomalies, using various forward and inverse techniques (Hood and Zakharian 2001; Arkani-Hamed 2001b; Frawley and Taylor 2004; Quesnel et al. 2007; Milburya et al. 2007; Langlais and Quesnel 2008).

3.3 The Moon, Venus and Mercury

Magnetic fields of near-lunar space, and the lunar surface, were first measured in the 1970's during the initial US-Soviet exploration of the Moon. Early measurements showed that the Moon has no global, core-generated magnetic field. Magnetometers, and early electron reflectometers, were place in low-inclination orbits and recognized the internal magnetic signature originating in the South Polar-Aitken basin region on the far side of the Moon. Magnetometers were carried on both US and Soviet landed vehicles, and measured fields of up to several hundred nT. The first global magnetic field measurement of the Moon was carried out by Lunar Prospector in 1998 and 1999, using both a magnetometer and an electron reflectometer (Binder 1998).

Lunar Prospector's magnetic field experiment was flown at low altitudes (30 km average altitude) between 19 December 1998 and 29 July 1999. The magnetometer was on a 2.5 m boom, and was a low-noise (6 pT RMS) triaxial vector fluxgate magnetometer that sampled at rates up to 18 Hz. Spin-averaged, calibrated, data was produced at 5 s intervals. All data are on NASA's Planetary Data System node. The fluxgate magnetometer senses three orthogonal components of the field at the spacecraft, while the electron reflectometer measures the magnitude of the magnetic field near the surface. Recent global maps of the internal magnetic field of the Moon include those of Purucker (2008) and Richmond and Hood (2008) using the vector fluxgate magnetometer, and the map of Mitchell et al. (2008) using the electron reflectometer.

The most detailed map (see Fig. 4) of the Lunar magnetic field is that of Purucker (2008) which describes the magnetic field to spherical degree 150, corresponding to wavelengths of 73 km. The map was made from radial and north–south horizontal components of the field measured in the lunar wake and tail regimes, after first removing a simple model of the external magnetic field. The technique involves isolating the correlative parts of three adjacent passes using a space domain formalism employing ESD (Purucker et al. 1996). This method allows for efficient field calculation and altitude normalization from relatively narrow N–S swaths, which are then assembled into a global mosaic. The density of the coverage was such that 99.2% of the one degree by one-half degree bins are populated, the remaining bins being in the polar regions.

Although Venus is often referred as the twin sister to the Earth, it does not possess an intrinsic magnetic field. The lack of a magnetic field is often interpreted as the result of a non convecting core inside Venus (Stevenson et al. 1983; Nimmo 2002). The surface of Venus is relatively young ($\sim$ .5 Gyr), and may be the result of a planet-scale resurfacing event (Stevenson 2003). The surface temperature of Venus (470°C) is below the Curie temperature of some magnetic minerals, but the titanium content deduced from X-ray fluorescence measurements made by Venera 13, 14 and Vega 2 (Fegley et al. 1997) suggests the presence of titanomagnetite, with associated lower Curie temperature. The lithospheric magnetic field of Venus, if any, is still yet to be detected.

The magnetic field of Mercury remains mysterious. Mariner 10 in 1974/5 reported evidences that Mercury possesses an internal magnetic field. It was measured to be as large as 400 nT at 330 km altitude (Ness et al. 1975). However, only two flybys were performed, opening a 30-year long debate on the origin of the Hermean magnetic field (Wicht

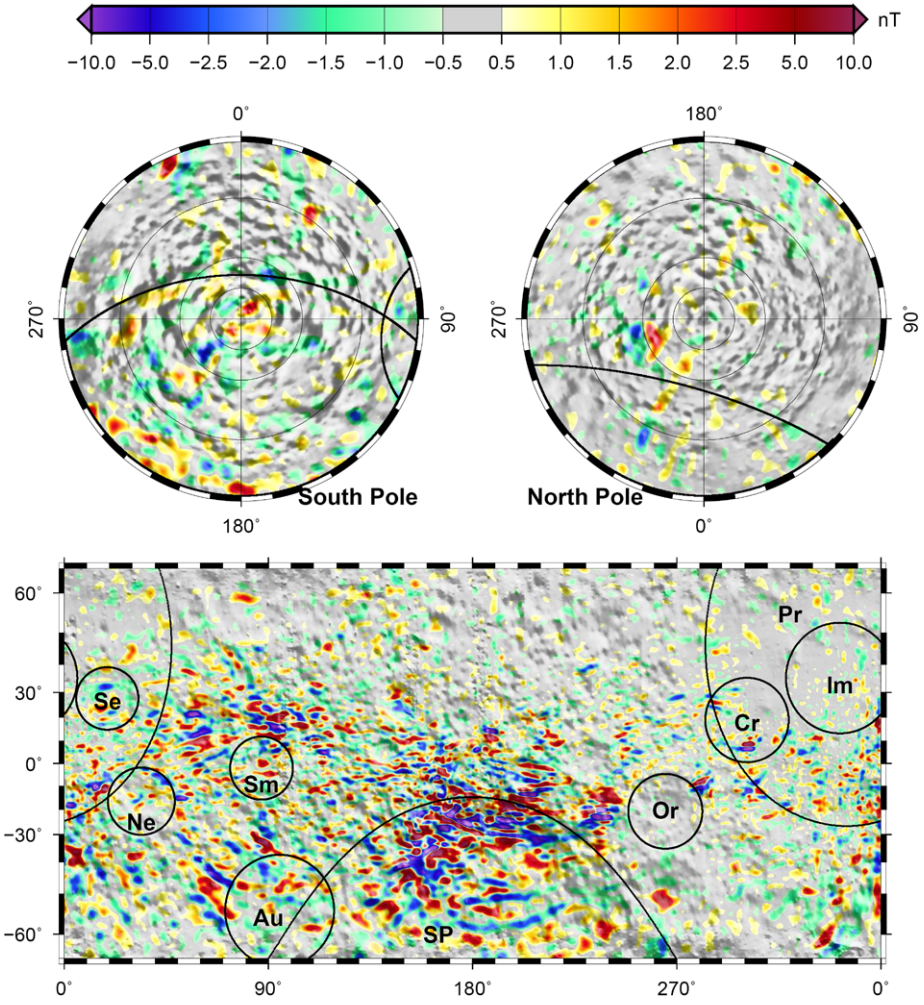

Fig. 4 Predicted radial component of the lunar magnetic field at an altitude of 30 km above the lunar mean radius, based on the spherical harmonic model of Purucker (2008), overlapped onto the ULCN lunar shaded relief. *Top*: South and North pole (orthographic projection), down to 60°S latitude. *Bottom*: Mercator projection between ±65°S latitude. The main rims of the largest impact basins are shown, with labels: Pr Procellarum, SP South Pole, Im Imbrium, Cr Crisium, Or Orientale, Au Australe, Ne Nectaris, Sm Smythii, and Se Serenitatis

et al. 2007). Many hypotheses were formulated, including thermoelectric dynamo (Stevenson 1987; Giampieri and Balogh 2002), or earth-like core dynamo acting under different conditions, with for instance a small inner core (Heimpel et al. 2005) or to the opposite a large inner core (Stanley et al. 2005; Takahashi and Matsushima 2006). Other explanations invoke a convection in a layered core, affecting only the innermost layer of the outer core (Christensen 2006). There may exist a lithospheric field on Mercury (Srnka 1976; Stephenson 1976; Aharonson et al. 2004), but flyby observations from the current MESSENGER mission (Anderson et al. 2008; Purucker et al. 2009) have yet to conclusively

observe a lithospheric magnetic field. The interested reader is referred to Anderson et al. (2009) for a detailed review on the Hermean magnetic field.

4 Origin(s) of the Crustal Field(s)

The Earth, the Moon and Mars present very different crustal magnetic fields, both in amplitude and in length scale. Their magnetic fields reflect the cumulative results of both magnetization and demagnetization processes which took place on these planets. In the following, we first discuss the remanent and the induced magnetization and then review the geodynamic properties and processes associated with large-scale magnetic signatures that possibly shaped the magnetic figure of these planets.

4.1 Remanent vs. Induced Origin?

On Mars and the Moon, the crustal magnetic field is primarily of remanent origin. On the Earth, to first order, most of the remanent magnetic contributions cancel out at large wavelength (i.e. those measurable at the spacecraft altitude), and the induced part dominates above continental domains.

The exact contribution of the remanent magnetization is actually difficult to estimate, unless the physical properties of the magnetic sources are known through rock sampling and analysis (Dunlop and Özdemir 2007). It is possible to estimate what is their relative contribution by using forward approaches. Global forward approaches mostly rely on the distribution of the vertically integrated magnetization. A simple estimate is based on the lateral magnetization contrast associated with the boundary between oceanic and continental domains. Counil et al. (1991) showed that abrupt boundaries between the thin oceanic crust (on average 7 km) and the thicker continental crust (on average 40 km) translates into a large scale magnetic signal which is present above the continental margins, and also above continental and oceanic basins. This does not suffice to explain all the observed magnetic anomalies. Taking into account the topography of the oceanic crust (Cohen and Achache 1994), as well as the oceanic remanent signature associated with the Cretaceous Quiet Zone (Dyment and Arkani-Hamed 1998), increases the correlation between forward predictions and actual observations. More complexity can be added to the forward modeling approach. Lateral thickness variations of the continental crust can be introduced as an initial parameter. This is what was done by Purucker et al. (2002). They computed the magnetic field associated with an *a priori* model of the magnetic crust, using a global seismic tomography model (Nataf and Ricard 1996) for the thickness of the crust completed by a sediment thickness model on top of it (Mooney et al. 1998). Two additional assumptions were made: (i) remanent magnetization is solely associated with oceanic crust, and (ii) relatively close susceptibility values for the continents and oceans (0.04 and 0.035 SI, respectively) were assumed (Purucker et al. 1998). The comparison of that forward predicted magnetic field (including terms between degrees 15 and 26) to those of MAGSAT and Ørsted-based models showed some differences in the location of some anomalies (see Fig. 5). These differences could of course be explained by unmodeled remanent contributions, but Purucker et al. (2002) instead suggested to shift the boundary between thick and thin magnetic layer inland, closer to the inboard Coastal plain boundary. The slightly corrected forward model then matched more closely actual observations.

The induced contribution is also the largest time-variable contribution of internal, non-core origin. In theory, it can be separated from the static remanent contribution, as pointed

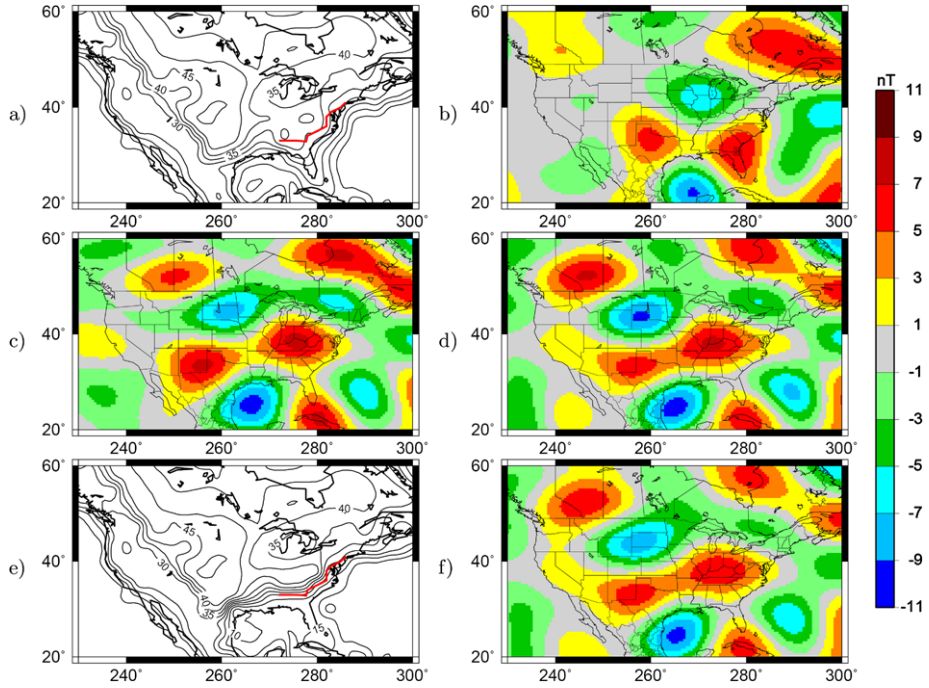

Fig. 5 (**a**) *A priori* thickness of the crust above the north American craton. The *solid red line* corresponds to the boundary between non-magnetic sediments of the Coastal Plain and more magnetic igneous and metamorphic continental rocks. (**b**) Predicted magnetic field at 400 km altitude from (**a**), between degrees 15 and 26. (**c**) and (**d**) 400-km altitude magnetic anomalies from MAGSAT-based and Ørsted-based models, respectively. Note the locations of the two positive lobes, centered above Kentucky and Texas, which differs from locations found in (**b**). (**e**) *A posteriori* thickness of the crust: main difference with (**a**) is the thinner thickness below Florida, Georgia and the rest of the Atlantic and Gulf Coastal Plains. (**f**) Predicted magnetic field at 400 km altitude from (**e**). After (Purucker et al. 2002)

by McLeod (1996): "crustal-source secular variation should dominate core-source secular variation for degrees greater than 22". This was recently challenged by Hulot et al. (2009), who showed that the time-varying crustal field is likely to hide the core field time variations beyond degree 18 or so. Lesur and Gubbins (2000) found that a time-dependent induced magnetic field would better explain the observed crustal biases than a static remanent field. Time variation of the crustal fields is predicted to be on average 0.06 to 0.12 $\mathrm{nT \cdot yr^{-1}}$ at the Earth's surface between degrees 15 and 90 (Thébault et al. 2009). In some places, it could reach up to 1.3 $\mathrm{nT \cdot yr^{-1}}$. Such a variation at spacecraft altitude would be lower, of the order of 0.02 $\mathrm{nT \cdot yr^{-1}}$, and therefore can not be directly detected without long time series of magnetic measurements. This crustal secular variation may for instance explain the difference observed between the observatory crustal biases (i.e. the non-core, lithospheric magnetic field at observatory locations) computed in 1980 and in 2000, using MAGSAT and Ørsted measurements (Mandea and Langlais 2002). The magnetic field of induced origin may indeed dominate the remanent magnetic field. These results, and others, make the remanent magnetic field of Mars even more intriguing, as the intensity of the remanent field on Mars exceeds by three orders of magnitude that of the Earth.

4.2 Impact Structures and Signatures

Impacts have been recognized as a major building and modifying process of planet's shapes and interiors. Impacts are usually associated with destructive effects, which depend on the size, velocity, trajectory angle and composition of the impactor, as well as on the nature of the impacted material. These parameters not only constrain the final shape of the crater (diameter, depth, single vs. complex crater), but also the peak pressure and the released energy associated with the impact. Their effects, as well as those associated with volcanoes and other deeper processes, can actually both (re-)magnetize and demagnetize rocks, through thermal, pressure or fracturing processes. The magnetic signature of an impact will therefore be different depending on whether it is emplaced while a core dynamo is active or not.

The pre-impact magnetization (if any) can be modified through mainly three processes. First, the impact is always associated with an excavation area, material being removed and spread away around the crater (Croft 1980). Second, the shock wave associated with the impact generates high pressures, which may demagnetize material, depending on their magnetic coercitivity (Cisowski and Fuller 1978). Such high pressures are also associated with local (re)magnetization processes (Gattacceca et al. 2008). Thermal effects are also possible, which will demagnetize (and possibly re-magnetize) those minerals which have a Curie temperature lower than the high temperatures associated with impacts. New minerals can also form, and acquire a magnetic remanence. Finally, impacts can cause plasmas, which may generate transient, very intense, magnetic fields (Crawford and Schultz 1999).

On the Earth, 176 impact structures have been identified so far (PASSC, Planetary and Space Science Centre 2009), ranging from 150 m to 300 km in diameter. This may be seen as a small number, especially when compared to other planets such as Mars or the Moon. But the identification of impact structures on the Earth is made difficult because of alteration processes. The largest conclusively identified impact structure, Vredefort, is located in South Africa. It is about 2.0 Ga old and is emplaced in a granitic basement. At the surface, magnetic fields are found to range between 10,000 and 75,000 nT, with horizontal gradients reaching a maximum of 9,000 $nT \cdot m^{-1}$ (Muundjua et al. 2007). Aeromagnetic surveys over this structure showed that magnetic anomalies range between $\pm$ 1500 nT at 300-m altitude (Corner and Wilsher 1989). These are mostly organized on a circular annulus, inside the crater rim as shown in Fig. 6. The very intense, small scale, magnetic fields found above Vredefort are very enigmatic, as this is highlighted by the extensive literature on the subject (see for instance (Reimold et al. 2008; Muundjua et al. 2008) for a recent debate). Most of the terrestrial craters exhibit magnetic anomalies weaker than their surroundings, with circular structures dominating (Grieve and Pilkington 1996). This is often interpreted as a local decrease in the magnetic susceptibility. However, this is not an absolute rule, and some craters are associated with magnetic highs. It must also be noted that none of the largest impact craters on the Earth (Vredefort, Chicxulub or Sudbury) produce magnetic signatures that are visible from orbit (see Fig. 2). It may also very well be that some of the observed large-scale magnetic anomalies are associated with subdued impact structures, as it has been suggested for Bangui (Central Africa), one of the largest (and yet unexplained) magnetic anomaly on the Earth (Girdler et al. 1992).

Magnetic effects of impact structures would theoretically be easier to study on other planets, because erosion effects have been less important, keeping a structure that is closer to the original one. But surface surveys are not possible, and one must rely on high altitude measurements. Comparison with terrestrial craters is therefore not directly possible.

Early studies of the lunar magnetic field suggested the importance of plasma-generated magnetic fields as the origin of observed magnetic anomalies (Gold and Sorer 1976). This

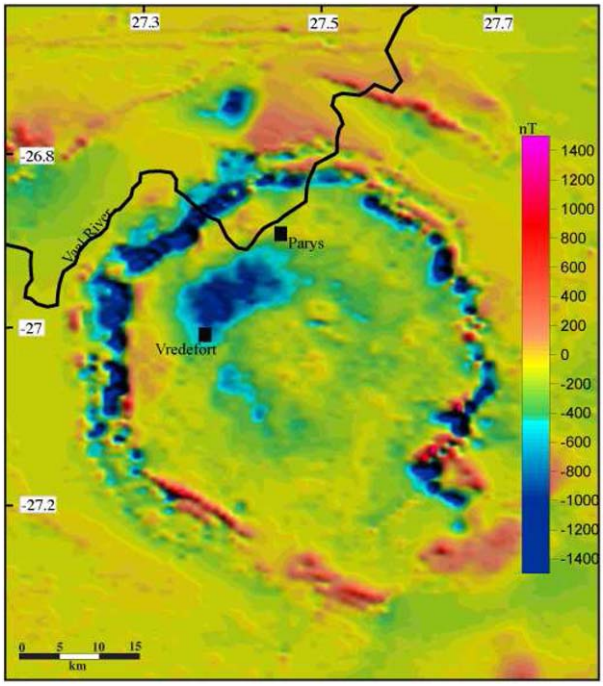

Fig. 6 Aeromagnetic anomaly map above Vredefort crater, at a nominal altitude of 150 m. Two partial circular features are visible, the outer one being located above iron-rich shales and the inner one above a facies transition. After (Muundjua et al. 2007)

is because lunar magnetic field are preferentially found on the antipodes to Crisium, Serenitatis, Imbrium, and Orientale basins (see Fig. 4). The strongest anomalies are actually found on the northwest edge of South Pole—Aitken crater, which is antipodal to Imbrium. Theoretical simulations (Hood and Huang 1991) showed that convergence of impact-related vapor clouds to the antipode of an impact can result into enhanced magnetic fields, if an ambient magnetic field existed at the time of the impact, of internal or external origin. Impacts are also associated with ejectas, which too converge to the antipodes. Although their thickness has been predicted to be small, they could contribute to a local increase of a preexisting magnetization (Hood and Artemieva 2008). This later would for instance be due to an ancient lunar paleodynamo, as this was recently suggested (Garrick-Bethell et al. 2009).

On Mars, the absence of magnetic field above the largest recognized impact structures (Hellas, Argyre, Isidis, see Fig. 3) has been interpreted as the proof that the core dynamo had already stopped at the time when this impacts took place (Acuña et al. 1999). This simplistic view is however incomplete, as craters are not isolated structures. More complexity comes from the secondary craters, associated with the largest impacts, which were suggested to be too associated with demagnetization processes (Artemieva et al. 2005). Studying the correlation between impact structures and magnetic fields requires some caution. Demagnetization effects often extend very far away from the crater rims, as this was suggested by Hood et al. (2003). For instance, pyrrhotite would loose about 50% of its magnetization under a 1 GPa pressure, which horizontally translates into 4 radii distance away from Hellas and Argyre (Rochette et al. 2003). Using different assumptions, Mohit and Arkani-Hamed (2004) concluded that only the area located inside the crater rims would be demagnetized, with partial demagnetization up to 1.4 radii away from the crater. The apparent demagnetization observed above large craters is used to estimate the time at which the dynamo stopped. Based on the magnetic signature of visible and buried impact structures (Frey 2008), Lillis

et al. (2008a) estimated that the dynamo ceased most likely 4.115–4.13 Ga ago, and that this cessation was rather rapid. Such a termination could be attributed to the Late Heavy Bombardment on Mars (Roberts et al. 2009). These different results highlight the importance of studying impact craters on other planets.

4.3 The Magnetic Signature of Other Processes

Many other processes can affect the creation, destruction, and mobilization of magnetic materials within the lithosphere of a planet. In the near surface, volcanism and related igneous processes such as dike emplacement, rifting, and faulting act to mobilize and create magnetic materials.

Generally speaking, magnetization is associated with minerals cooling down below their Curie temperature in the presence of a magnetic field. On the Earth, the magnetic signature associated with seafloor spreading has been recognized for a long time (Vine and Matthews 1963). This signature is used to constrain and reconstruct plate tectonic patterns. On Mars, a sea-floor spreading like scenario was proposed to explain the southern hemisphere intense anomalies (Connerney et al. 1999). Transformed faults have also been suggested in Terra Meridiani (Connerney et al. 2005), but other elements associated with plate tectonics such as subduction zones have yet not been identified. Remote magnetic measurements made above volcanic constructs can be used to estimate the magnetic properties of a volcano (Parker et al. 1987). Taking into account the precise shape of the structure, as well as information obtained from other techniques such as drilling, can help to understand the structure of the underlying volcano (Blanco-Montenegro et al. 2007). Such studies are also useful to constrain the behavior of the paleodynamo. Volcanic edifices and associated magnetic signatures are also studied on Mars, whether they are magnetized, like Apollinaris Patera (Langlais and Purucker 2007), or not, like Hadriaca Patera (Lillis et al. 2008b). Recently, the magnetic field around Arsia Mons volcano was analyzed. Results suggested an important intrusive regime, required to explain the partial demagnetization (Lillis et al. 2009).

Deeper processes can also be characterized through their magnetic signature. This is the case for granulite-grade metamorphism (Clark 1997), and for serpentinization. This later is recognized as an important source for secondary magnetization. It is a metamorphic reaction, occurring at low-to-medium temperature and low pressure. It corresponds to the hydration of mafic or ultramafic rocks of the crust and mantle, and produces serpentine, and other minerals such as talc, quartz or magnetite. The newly formed magnetite acquires a stable remanent magnetization in the presence of an intense magnetic field. On the Earth, serpentinization is commonly found at mid-ocean ridges (Mével 2003). Fresh basalts are rapidly altered, which may reduce the initial thermoremanent magnetization, but the chemical remanent magnetization associated with new minerals could contribute to as much as 80% of the observed magnetic anomalies (Raymond and Labrecque 1987). Serpentinization is one of the processes that is suggested as the origin of the intense Martian magnetic field anomalies (Hood et al. 2005), it is also invoked to explain the crustal dichotomy (Quesnel et al. 2009). Another setting for serpentinization reaction is the mantle wedge of subduction where water is released from the subducted cooler crust. On the Earth the lithospheric magnetic field anomalies observed above the Cascadia subduction zone (Fig. 7) were interpreted by a hydrated mantle, this hypothesis being also supported by gravity field interpretations and seismic velocities (Blakely et al. 2005). Unaltered subdued material can also increase the thickness of the magnetized layer, as this was suggested above the Sumatra subduction area (Purucker and Ishihara 2005; Mandea and Thébault 2007).

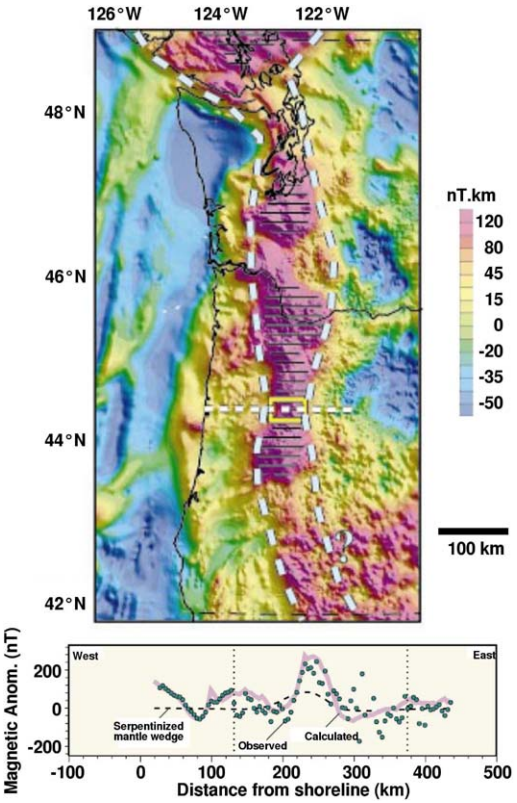

Fig. 7 *Top*: aeromagnetic anomalies (transformed to magnetic potential in nT·km) above the Cascadia subduction zone. *Black horizontal line* pattern shows location of the most intense magnetic anomalies. The *white East–West dashed line* is the location of a teleseismic transect, showing evidence of serpentinized forearc mantle (*yellow rectangle*). *Light blue dashed line* bounds magnetic anomalies interpreted as partially caused by hydrated mantle. *Bottom*: stacked magnetic profiles and predicted magnetic field associated to the Oregon forearc model. *Vertical dotted lines* demotes location of the teleseismic transect. Also shown the magnetic field associated with the mantle wedge alone. Adapted from (Blakely et al. 2005)

5 Conclusions and Open Issues

The magnetic signature of the lithosphere of the telluric planets and of the Moon is related to all the processes that affected and shaped the figure of these planets. The Earth, the Moon, Mars, Venus and Mercury present five different magnetic faces, with overlapping induced and remanent contributions, a weak remanent field of uncertain origin, a strong remanent field very likely related to a past dynamo, a lack of (so far) detectable magnetic field, and a possibly weak lithospheric component overlapped by a weak dynamo field, respectively.

It is recognized that magnetization within these telluric planets and the Moon is controlled in part by the amount of available iron within the crust. Iron is partitioned among oxide, sulfide, and silicate phases in the crust (Clark 1997), and only the first and second of these phases can retain significant remanent or induced magnetization. The relationship between iron abundance and minimum magnetization can be estimated, using techniques developed by Parker (2003). Results are shown on Fig. 8, assuming a 40-km thick magnetized layer. There is a broad correlation between crustal iron content and magnetization for Mars, the Earth and Moon. Venus, and to some extent, Mercury, may appear as anomalous. But the assumed 40-km thick magnetized layer for these two planets is probably wrong by a factor of magnitude; more realistic values would increase the magnetization contrast by a similar factor. Additional influences on the magnetization include the strength of the dynamo field in which the magnetization was acquired, and the mineralogy of the magnetic phases.

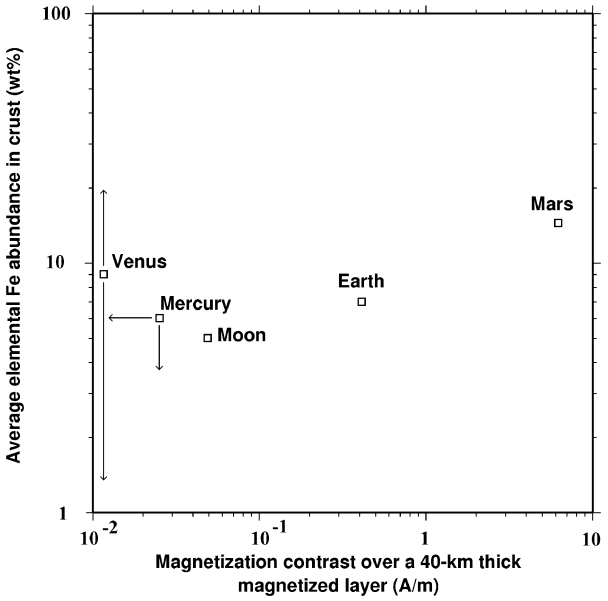

Fig. 8 Minimum magnetization contrast (A/m) versus Fe content of crust (wt%) for the Earth, Mars, Moon, Mercury and Venus, assuming a 40-km-thick magnetized layer. Fe content taken from Hahn et al. (2007), Lodders and Fegley (1998), Grimm and Hess (1997), Solomon et al. (2008). *Arrows on Mercury* indicate that upper bounds for Fe content and magnetization contrast are considered. *Arrows on Venus* indicate the poorly constrained Fe content. Adapted from (Purucker et al. 2009)

The magnetic field of lithospheric origin has a different behavior close to the surface or at spacecraft altitude. Simply imagine the Earth (or its twin) without a dynamo: a MGS-like spacecraft would have measured very little magnetic fields, if any! It is mandatory to pursue our efforts in measuring, modeling and interpreting the magnetic field at various wavelength on the Earth and on other planets.

On the Earth, the WDMAM 2.0 is currently in progress; improvements will be made with the addition of both surface and spacecraft measurements. This will be possible thanks to the forthcoming ESA's Swarm mission, a novel constellation comprising three identical satellites carrying magnetometers. Two of the Swarm satellites will fly close to each other at lower altitudes, measuring the East–West gradient of the magnetic field, while the third one will fly at a higher altitude (Friis-Christensen et al. 2006). These further improvements in describing and understanding the magnetic field anomaly source properties will also benefit from joint analysis of geophysical and geological datasets.

The flying NASA MESSENGER mission, and the planned ESA's Bepi Colombo mission will characterize the Hermean magnetic field, and possibly put limits on the lithospheric field of Mercury. On Mars, following the surprising discovery of Mars crustal magnetism by MGS in 1996, ten more spacecraft and landers have been launched with no experiment capable of measuring magnetic fields, with the exception of Rosetta which made one flyby close to Mars in 2007 (Boesswetter et al. 2009). Hopefully, the next NASA's SCOUT mission, MAVEN, will provide new measurements of the Martian magnetic field. Such measurements, combined with monitoring of the current atmospheric escape on Mars (Langlais et al. 2009; Leblanc et al. 2009) could be used to estimate what has been the fate of water on Mars along its past history.

More than 400 year ago, Gilbert concluded from his observations that the compass was deviated by "imperfections" (i.e. oceanic areas or continental masses) on the sphere. Now we know that the deviation of a compass is related to changes in the magnetic content, whether it is the magnetization components or the amount of magnetized material. The next

step will be to evaluate which one of these two properties governs the magnetic signature of the lithosphere of terrestrial planets.

Acknowledgements All geographical figures were produced with GMT (Wessel and Smith 1991). Support was provided by Helmholtz-Zentrum Potsdam Deutsches GeoForschungsZentrum, Germany; Institut National des Sciences de la Terre/CNRS, France. We would like to thank E. Thébault for discussions on Spherical Cap Harmonic Analysis, R. Hart for providing figure on Vredefort crater, R. Balogh and the staff at ISSI for organizing a fruitful workshop. This work is dedicated to the memory of Mario H. Acuña, who inspired so many of us.

References

M.H. Acuña, J.E.P. Connerney, P. Wasilewski, R.P. Lin, K.A. Anderson, C.W. Carlson, J. McFadden, D.W. Curtis, H. Réme, A. Cros, J.L. Médale, J.A. Sauvaud, C. d'Uston, S.J. Bauer, P. Cloutier, M. Mayhew, N.F. Ness, Mars Observer magnetic fields investigation. J. Geophys. Res. **97**, 7799–7814 (1992)

M.H. Acuña, J.E.P. Connerney, N.F. Ness, R.P. Lin, D. Mitchell, C.W. Carlson, J. McFadden, K.A. Anderson, H. Reme, C. Mazelle, D. Vignes, P. Wasilewski, P. Cloutier, Global distribution of crustal magnetization discovered by the Mars global surveyor MAG/ER experiment. Science **284** (1999). doi:10.1126/science.284.5415.790

M.H. Acuña, J.E.P. Connerney, P. Wasilewski, R.P. Lin, D. Mitchell, K.A. Anderson, C.W. Carlson, J. McFadden, H. Rème, C. Mazelle, D. Vignes, S.J. Bauer, P. Cloutier, N.F. Ness, Magnetic field of Mars: Summary of results from the aerobraking and mapping orbits. J. Geophys. Res. **106** (2001). doi:10.1029/2000JE001404

O. Aharonson, M.T. Zuber, S.C. Solomon, Crustal remanence in an internally magnetized non-uniform shell: a possible source for Mercury's magnetic field? Earth Planet. Sci. Lett. **218**, 261–268 (2004)

A.L. Albee, R.E. Arvidson, F. Palluconi, T. Thorpe, Overview of the Mars global surveyor mission. J. Geophys. Res. **106** (2001). doi:10.1029/2000JE001306

B.J. Anderson, M.H. Acuña, H. Korth, M.E. Purucker, C.L. Johnson, J.A. Slavin, S.C. Solomon, R.L. McNutt, The structure of Mercury's magnetic field from MESSENGER's first flyby. Science **321**, 82–85 (2008). doi:10.1126/science.1159081

Anderson et al., Space Sci. Rev. (2009, this issue)

J. Arkani-Hamed, A 50-degree spherical harmonic model of the magnetic field of Mars. J. Geophys. Res. **106** (2001a). doi:10.1029/2000JE001365

J. Arkani-Hamed, Paleomagnetic pole positions and pole reversals of Mars. Geophys. Res. Lett. **28** (2001b). doi:10.1029/2001GL012928

J. Arkani-Hamed, A coherent model of the crustal magnetic field of Mars. J. Geophys. Res. **109** (2004). doi:10.1029/2004JE002265

N. Artemieva, L.L. Hood, B.A. Ivanov, Impact demagnetization of the Martian crust: Primaries versus secondaries. Geophys. Res. Lett. **32** (2005). doi:10.1029/2005GL024385

Baumjohann et al., Space Sci. Rev. (2009, this issue)

A.B. Binder, Lunar Prospector: Overview. Science **281**, 1475–1476 (1998)

R.J. Blakely, *Potential Theory in Gravity and Magnetic Applications* (Cambridge University Press, Cambridge, 1995), p. 441

R.J. Blakely, T.M. Brocher, R.E. Wells, Subduction zone magnetic anomalies and implications for hydrated forearc mantle. Geology **33**, 445–448 (2005)

I. Blanco-Montenegro, R. De Ritis, M. Chiappini, Imaging and modelling the subsurface structure of volcanic calderas with high-resolution aeromagnetic data at vulcano (Aeolian islands, Italy). Bull. Volcanol. **69** (2007). doi:10.1007/s00445-006-0100-7

A. Boesswetter, U. Auster, I. Richter, M. Fränz, B. Langlais, S. McKenna-Lawlor, S. Simon, U. Motschmann, K.H. Glassmeier, N.J.T. Edberg, R. Lundin, Rosetta swing-by at Mars - An analysis of the ROMAP measurements in comparison with results of 3d multi-ion hybrid simulations and MEX/ASPERA-3 data. Ann. Geophys. **27**, 2383–2398 (2009)

J.C. Cain, D.R. Schmitz, L. Muth, Small-scale features in the Earth's magnetic field observed by Magsat. J. Geophys. Res. **89**, 1070–1076 (1984)

J.C. Cain, B.B. Ferguson, D. Mozzoni, An $n = 90$ internal potential function of the Martian crustal magnetic field. J. Geophys. Res. **108** (2003). doi:10.1029/2000JE001487

A. Chambodut, I. Panet, M. Mandea, M. Diament, M. Holschneider, O. Jamet, Wavelet frames: an alternative to spherical harmonic representation of potential fields. Geophys. J. Int. **163** (2005). doi:10.1111/j.1365-246X.2005.02754.x

U.R. Christensen, A deep dynamo generating Mercury's magnetic field. Nature **444** (2006). doi:10.1038/nature05342
S.M. Cisowski, M. Fuller, The effect os shock on the magnetism of terrestrial rocks. J. Geophys. Res. **83**, 3441–3458 (1978)
D. Clark, Magnetic petrophysics and magnetic petrology: aids to geological interpretation of magnetic surveys. AGSO J. Aust. Geol. Geophys. **2**, 83–103 (1997)
Y. Cohen, J. Achache, Contribution of induced and remanent magnetization to long-wavelength oceanic magnetic anomalies. J. Geophys. Res. **99**, 2943–2954 (1994)
F.R. Colomb, C. Alonso, C. Hofmann, I. Nollmann, SAC-C mission, an example of international cooperation. Adv. Space Res. **34** (2004). doi:10.1016/j.asr.2003.10.039
J.E.P. Connerney, M.H. Acuna, P.J. Wasilewski, N.F. Ness, H. Reme, C. Mazelle, D. Vignes, R.P. Lin, D.L. Mitchell, P.A. Cloutier, Magnetic lineations in the ancient crust of Mars. Science **284**, 794 (1999)
J.E.P. Connerney, M.H. Acuña, P.J. Wasilewski, G. Kletetschka, N.F. Ness, H. Rème, R.P. Lin, D.L. Mitchell, The global magnetic field of Mars and implications for crustal evolution. Geophys. Res. Lett. **28** (2001). doi:10.1029/2001GL013619
J.E.P. Connerney, M.H. Acuña, N.F. Ness, T. Spohn, G. Schubert, Mars crustal magnetism. Space Sci. Rev. **111** (2004). doi:10.1023/B:SPAC.0000032719.40094.1d
J.E.P. Connerney, M.H. Acuña, N.F. Ness, G. Kletetschka, D.L. Mitchell, R.P. Lin, H. Reme, Tectonic implications of Mars crustal magnetism. Proc. Nat. Acad. Sci. **102** (2005). doi:10.1073/pnas.0507469102
B. Corner, W.A. Wilsher, Structure of the Witwatersrand basin derived from interpretation of aeromagnetic and gravity data. Exploration '87 Geol. Surv. Can. Spec. **3**, 523–546 (1989)
J. Counil, Y. Cohen, J. Achache, The global continent-ocean magnetization contrast. Earth Planet. Sci. Lett. **103**, 354–364 (1991)
D.A. Crawford, P.H. Schultz, Electromagnetic properties of impact-generated plasma, vapor and debris. Int. J. Impact Eng. **23**, 169–180 (1999)
S.K. Croft, Cratering flow fields – Implications for the excavation and transient expansion stages of crater formation, in *Proc. Lunar Planet. Sci. Conf.*, vol. 11, 1980, pp. 2347–2378
S.S. Dolginov, L.N. Zhuzgov, The magnetic field and magnetosphere of the planet Mars. Planet. Space Sci. **39**, 1493–1510 (1991)
S.S. Dolginov, L.N. Zhuzgov, N.V. Pushkov, Preliminary report on geomagnetic measurements on the third Soviet artificial Earth satellite. Planet. Space Sci. **5**, 244–247 (1961)
D.J. Dunlop, O. Özdemir, *Rock Magnetism: Fundamentals and Frontiers* (Cambridge University Press, Cambridge, 1997), p. 573
D.J. Dunlop, O. Özdemir, Magnetizations of rocks and minerals, in *Treatise on Geophysics*, vol. 5, ed. by M. Kono (Elsevier, Amsterdam, 2007), pp. 277–336
J. Dyment, J. Arkani-Hamed, Equivalent source magnetic dipoles revisited. Geophys. Res. Lett. **25**, 2003–2006 (1998)
J. Dyment, S.C. Cande, J. Arkani-Hamed, Skewness of marine magnetic anomalies created between 85 and 40 Ma in the Indian ocean. J. Geophys. Res. **99**, 24121–24134 (1995)
ETOPO5, Data Announcement 88-MGG-02, Digital relief of the surface of the Earth. NOAA. National Geophysical Data Center, Boulder, Colorado, USA (1988)
B.J. Fegley, G. Klingelhfer, K. Lodders, T. Widemann, Geochemistry of surface-atmosphere interactions on Venus, in *Venus II*, ed. by W. Boucher, D. Hunten, R. Phillips (Univ. of Arizona Press, Tucson, 1997), pp. 591–636
J.J. Frawley, P.T. Taylor, Paleo-pole positions from martian magnetic anomaly data. Icarus **172**, 316–327 (2004)
H.V. Frey, Ages of very large impact basins on Mars: Implications for the late heavy bombardment in the inner solar system. Geophys. Res. Lett. (2008). doi:10.1029/2008GL033515
E. Friis-Christensen, H. Lühr, G. Hulot, A constellation to study the Earth's magnetic field. Earth Planets Space **58**, 351–358 (2006)
I. Garrick-Bethell, B.P. Weiss, D.L. Shuster, J. Buz, Early lunar magnetism. Science **323** (2009). doi:10.1126/science.1166804
J. Gattacceca, L. Berthe, M. Boustie, F. Vadeboin, P. Rochette, T. de Resseguier, On the efficiency of shock magnetization processes. Phys. Earth Planet. Int. **166** (2008). doi:10.1016/j.pepi.2007.09.005
G. Giampieri, A. Balogh, Mercury's thermoelectric dynamo model revisisted. Planet. Space Sci. **50**, 757–762 (2002)
W. Gilbert, *De magnete* (Translation by Silvanus Phillips Thompson and the Gilbert Club, Chiswick Press, 1900, 337 pp., London, UK, 1600)
R.W. Girdler, P. Taylor, J.J. Frawley, A possible impact origin for the Bangui magnetic anomaly (Central Africa). Tectonophysics **212**, 45–58 (1992)
T. Gold, S. Sorer, Cometary impact and the magnetization of the Moon. Planet. Space Sci. **24**, 45–54 (1976)

R.A.F. Grieve, M. Pilkington, The signature of terrestrial impacts. AGSO J. Geol. Geophys. **16**, 399–420 (1996)
R.E. Grimm, P.C. Hess, The crust of Venus, in *Venus II*, ed. by W. Boucher, D. Hunten, R. Phillips (Univ. of Arizona Press, Tucson, 1997), pp. 1205–1244
B.C. Hahn, S.M. McLennan, G.J. Taylor, W.V. Boynton, J.M. Dohn, M.J. Finch, D.K. Hamara, D.M. Janes, S. Karunatillake, J.M. Keller, K.E. Kerry, A.E. Metzger, R.M.. Williams, Mars Odyssey Gamma Ray Spectrometer elemental abundances and apparent relative surface age: implications for Martian crustal evolution. J. Geophys. Res. **112** (2007). doi:10.1029/2006JE002821
G.V. Haines, Spherical cap harmonic analysis. J. Geophys. Res. **90**, 2583–2591 (1985)
M.H. Heimpel, J.M. Aurnou, F.M. Al-Shamali, N. Gomez Perez, A numerical study of dynamo action as a function of spherical shell geometry. Earth Planet. Sci. Lett. **236** (2005). doi:10.1016/j.epsl.2005.04.032
L.L. Hood, N.A. Artemieva, Antipodal effects of lunar basin-forming impacts: initial 3D simulations and comparisons with observations. Icarus **193** (2008). doi:10.1016/j.icarus.2007.08.023
L.L. Hood, Z. Huang, Formation of magnetic anomalies antipodal to lunar impact basins – Two-dimensional model calculations. J. Geophys. Res. **96**, 9837–9846 (1991)
L.L. Hood, A. Zakharian, Mapping and modeling of magnetic anomalies in the northern polar region of Mars. J. Geophys. Res. **106** (2001). doi:10.1029/2000JE001304
L.L. Hood, N.C. Richmond, E. Pierazzo, P. Rochette, Distribution of crustal magnetic fields on Mars: Shock effects of basin-forming impacts. Geophys. Res. Lett. **30** (2003). doi:10.1029/2002GL016657
L.L. Hood, C.N. Young, N.C. Richmond, K.P. Harrison, Modeling of major martian magnetic anomalies: Further evidence for polar reorientations during the Noachian. Icarus **177** (2005). doi:10.1016/j.icarus.2005.02.008
Hulot et al., Space Sci. Rev. (2009, this issue)
G. Hulot, N. Olsen, E. Thébault, K. Hemant, Crustal concealing of small scale core field secular variation. Geophys. J. Int. **177** (2009). doi:10.1111/j.1365-246X.2009.04119.x
J. Jankowski, C. Sucksdorff, *Guide for Magnetic Measurements and Observatory Practice* (Int. Assoc. Geomag. Aeronomy, Warsaw, 1996), p. 235
J.V. Korhonen, J.D. Fairhead, M. Hamoudi, K. Hemant, V. Lesur, M. Mandea, S. Maus, M.E. Purucker, D. Ravat, T. Sazonova, E. Thébault, Magnetic anomaly map of the world—Carte des anomalies magnétiques du monde, Scale: 1:50,000,000, 1st edition. Commission for the Geological Map of the World (2007)
R.A. Langel, Global magnetic anomaly maps derived from POGO spacecraft data. Phys. Earth Planet. Int. **62**, 208–230 (1990)
B. Langlais, M.E. Purucker, A polar magnetic paleopole associated with Apollinaris Patera. Planet. Space Sci. **55** (2007). doi:10.1016/j.pss.2006.03.008
B. Langlais, Y. Quesnel, New perspectives on Mars' crustal magnetic field. Comptes Rendus Geosci. **340** (2008). doi:10.1016/j.crte.2008.08.006e
B. Langlais, M.E. Purucker, M. Mandea, Crustal magnetic field of Mars. J. Geophys. Res. **109** (2004). doi:10.1029/2003JE002048
B. Langlais, F. Leblanc, T. Fouchet, S. Barabash, D. Breuer, E. Chassefière, A. Coates, V. Dehant, F. Forget, H. Lammer, S. Lewis, M. Lopez-Valverde, M. Mandea, M. Menvielle, A. Pais, M. Paetzold, P. Read, C. Sotin, P. Tarits, S. Vennerstrom, G. Branduardi-Raymont, G. Cremonese, J.G.M. Merayo, T. Ott, H. Rème, J.G. Trotignon, J.E. Walhund, Mars Environment and Magnetic Orbiter: model payload. Exp. Astron. **22** (2009). doi:10.1007/s10686-008-9101-1
F. Leblanc, B. Langlais, T. Fouchet, S. Barabash, D. Breuer, E. Chassefière, A. Coates, V. Dehant, F. Forget, H. Lammer, S. Lewis, M. Lopez-Valverde, M. Mandea, M. Menvielle, A. Pais, M. Paetzold, P. Read, C. Sotin, P. Tarits, S. Vennerstrom, Mars environment and magnetic orbiter: Science and measurement objectives. Astrobiology (2009). doi:10.1089/AST.2007.022
V. Lesur, Introducing localized constraints in global geomagnetic field modelling. Earth Planets Space **58**, 477–483 (2006)
V. Lesur, D. Gubbins, Using geomagnetic secular variation to separate remanent and induced sources of the crustal magnetic field. Geophys. J. Int. **142**, 889–897 (2000)
V. Lesur, A. Jackson, Exact solutions for internally induced magnetization in a shell. Geophys. J. Int. **140**, 453–459 (2000)
V. Lesur, S. Maus, A global lithospheric magnetic field model with reduced noise level in the polar regions. Geophys. Res. Lett. **33** (2006). doi:10.1029/2006GL025826
V. Lesur, I. Wardinski, M. Rother, M. Mandea, GRIMM: the GFZ Reference Internal Magnetic Model based on vector satellite and observatory data. Geophys. J. Int. **173** (2008). doi:10.1111/j.1365-246X.2008.03724.x
R.J. Lillis, H.V. Frey, M. Manga, Rapid decrease in Martian crustal magnetization in the Noachian era: Implications for the dynamo and climate of early Mars. Geophys. Res. Lett. **35** (2008a). doi:10.1029/2008GL034338

R.J. Lillis, H.V. Frey, M. Manga, D.L. Mitchell, R.P. Lin, M.H. Acuña, S.W. Bougher, An improved crustal magnetic field map of Mars from electron reflectometry: Highland volcano magmatic history and the end of the martian dynamo. Icarus **194** (2008b). doi:10.1016/j.icarus.2007.09.032

R.J. Lillis, J. Dufek, J.E. Bleacher, M. Manga, Demagnetization of crust by magmatic intrusion near the arsia mons volcano: Magnetic and thermal implications for the development of the tharsis province, mars. J. Volcanol. Geotherm. Res. (2009, in press). doi:10.1016/j.jvolgeores.2008.12.007

K. Lodders, J.B. Fegley, *The Planetary Scientist's Companion* (Oxford University Press, New York, 1998), p. 371

P. Lognonné, J. Gagnepain-Beyneix, H. Chenet, A new seismic model of the Moon: implications for structure, thermal evolution and formation of the Moon. Earth Planet. Sci. Lett. **211** (2003). doi:10.1016/S0012-821X(03)00172-9

M. Mandea, B. Langlais, Observatory crustal magnetic biases during MAGSAT and Ørsted satellite missions. Geophys. Res. Lett. **29** (2002). doi:10.1029/2001GL013693

M. Mandea, M.E. Purucker, Observing, modeling, and interpreting magnetic fields of the solid Earth. Surv. Geophys. **26** (2005). doi:10.1007/s10712-005-3857-x

M. Mandea, E. Thébault, *The Changing Faces of the Earth's Magnetic Field* (Commission for The Geological Map of the World, France, 2007), p. 49

S. Maus, V. Haak, Magnetic field annihilators: invisible magnetization at the magnetic equator. Geophys. J. Int. **155**, 509–513 (2003)

S. Maus, M. Rother, R. Holme, H. Lühr, N. Olsen, V. Haak, First scalar magnetic anomaly map from champ satellite data indicates weak lithospheric field. Geophys. Res. Lett. **29** (2002). doi:10.1029/2001GL013685

S. Maus, H. Lühr, M. Rother, K. Hemant, G. Balasis, P. Ritter, C. Stolle, Fifth-generation lithospheric magnetic field model from CHAMP satellite measurements. Geochem., Geophys., Geosyst. **8** (2007). doi:10.1029/2006GC001521

S. Maus, F. Yin, H. Lühr, C. Manoj, M. Rother, J. Rauberg, I. Michaelis, C. Stolle, R.D. Müller, Resolution of direction of oceanic magnetic lineations by the sixth-generation lithospheric magnetic field model from CHAMP satellite magnetic measurements. Geochem., Geophys., Geosyst. **9** (2008). doi:10.1029/2008GC001949

C. Mayer, T. Maier, Separating inner and outer Earth's magnetic field from CHAMP satellite measurements by means of vector scaling functions and wavelet. Geophys. J. Int. **167** (2006). doi:10.1111/j.1365-246X.2006.03199.x

M.A. Mayhew, Inversion of satellite magnetic anomaly data. J. Geophys. **45**, 119–128 (1979)

M.G. McLeod, Spatial and temporal power spectra of the geomagnetic field. J. Geophys. Res. **101**, 2745–2763 (1996)

C. Mével, Serpentinization of abyssal peridotites at mid-ocean ridges. Comptes Rendus Geosci. **335**, 825–852 (2003). doi:10.1016/j.crte.2003.08.006

C.A.E. Milburya, S.E. Smrekar, C.A. Raymond, G. Schubert, Lithospheric structure in the eastern region of Mars' dichotomy boundary. Planet. Space Sci. **55** (2007). doi:10.1016/j.pss.2006.03.009s

D.L. Mitchell, R.P. Lin, C. Mazelle, H. Rème, P.A. Cloutier, J.E.P. Connerney, M.H. Acuña, N.F. Ness, Probing Mars' crustal magnetic field and ionosphere with the MGS Electron Reflectometer. J. Geophys. Res. **106** (2001). doi:10.1029/2000JE001435

D.L. Mitchell, R.J. Lillis, R.P. Lin, J.E.P. Connerney, M.H. Acuña, A global map of Mars' crustal magnetic field based on electron reflectometry. J. Geophys. Res. **112** (2007). doi:10.1029/2005JE002564

D.L. Mitchell, J.S. Halekas, R.P. Lin, S. Frey, L.L. Hood, M.H. Acuña, A. Binder, Global mapping of lunar crustal magnetic fields by Lunar Prospector. Icarus **194** (2008). doi:10.1016/j.icarus.2007.10.027

D. Moehlmann, The question of a Martian planetary magnetic field. Adv. Space Res. **12**, 213–217 (1992)

D. Moehlmann, W. Riedler, J. Rustenbach, K. Schwingenschuh, J. Kurths, U. Motschmann, T. Roatsch, K. Sauer, H.T.M. Lichtenegger, The question of an internal Martian magnetic field. Planet. Space Sci. **39**, 83–88 (1991)

P.S. Mohit, J. Arkani-Hamed, Impact demagnetization of the martian crust. Icarus **168** (2004). doi:10.1016/j.icarus.2003.12.005

W.D. Mooney, G. Laske, T.G. Masters, CRUST 5.1: A global crustal model at 5 degrees x 5 degrees. J. Geophys. Res. **103**, 727–747 (1998)

M. Muundjua, R.J. Hart, S.A. Gilder, L. Carporzen, A. Galdeano, Magnetic imaging of the vredefort impact crater, south Africa. Earth Planet. Sci. Lett. **261** (2007). doi:10.1016/j.epsl.2007.07.044

M. Muundjua, A. Galdeano, L. Carporzen, S.A. Gilder, R.J. Hart, M.A.G. Andreoli, M. Tredoux, Reply to scientific comment by W.U. Reimold, R.L. Gibson and H. Henkel on Muundjua et al. (2007), magnetic imaging of the vredefort impact crater, south Africa, epsl 261, pp. 456–468. Earth Planet. Sci. Lett. **273** (2008). doi:10.1016/j.epsl.2008.06.044

H.C. Nataf, Y. Ricard, 3SMAC: An a priori tomographic model of the upper mantle based on geophysical modeling. Phys. Earth Planet. Int. **95**, 101–122 (1996)
J. Needham, Science and civilisation in China, vol. 4 *Physics and Physical Technology*, Part 1 *Physics* (Cambridge University Press, Cambridge, 1962), pp. 314–334
N.F. Ness, The magnetic fields of Mercury, Mars, and moon. Ann. Rev. Earth Planet. Sci. **7**, 249–288 (1979)
N.F. Ness, K.W. Behannon, R.P. Lepping, Y.C. Whang, Magnetic field of Mercury confirmed. Nature **255**, 204 (1975)
F. Nimmo, Why does Venus lack a magnetic field? Geology **30**, 989–990 (2002)
N. Olsen, R. Holme, G. Hulot, T. Sabaka, T. Neubert, L. Toffner-Clausen, F. Primdahl, J. Jorgensen, J.-M. Leger, D. Barraclough, J. Bloxham, J. Cain, C. Constable, V. Golovkov, A. Jackson, P. Kotze, B. Langlais, S. Macmillan, M. Mandea, J. Merayo, L. Newitt, M. Purucker, T. Risbo, M. Stampe, A. Thomson, C. Voorhies, Orsted initial field model. Geophys. Res. Lett. **27**(22), 3607–3610 (2000)
N. Olsen, M. Mandea, Rapidly changing flows in the Earth's core. Nature Geosci. **1** (2008). doi:10.1038/ngeo203
R.L. Parker, Ideal bodies for Mars magnetics. J. Geophys. Res. **108** (2003). doi:10.1029/2001JE001760
R.L. Parker, L. Shure, J.A. Hildebrand, The application of inverse theory to seamount magnetism. Rev. Geophys. **25**, 17–40 (1987)
PASSC, Planetary and Space Science Centre, *Earth impact database*, 2009. http://www.unb.ca/passc/impactdatabase/
V.G. Perminov, The Difficult Road to Mars: A Brief History of Mars Exploration in the Soviet Union (Monographs in aerospace history; no. 15, NASA Headquarters, Washington, D.C., 1999)
M.E. Purucker, A global model of the internal magnetic field of the Moon based on Lunar Prospector magnetometer observations. Icarus **197** (2008). doi:10.1016/j.icarus.2008.03.016
M.E. Purucker, T. Ishihara, Magnetic images of the Sumatra region crust. EOS, Trans. Am. Geophys. Union **86** (2005). doi:10.1029/2005EO100002
M.E. Purucker, K. Whaler, Crustal magnetism, in *Treatise on Geophysics*, vol. 5, Geomagnetism, ed. by M. Kono (Elsevier, Amsterdam, 2007), pp. 195–237
M.E. Purucker, T.J. Sabaka, R.A. Langel, Conjugate gradient analysis: A new tool for studying satellite magnetic data sets. Geophys. Res. Lett. **23**, 507–510 (1996)
M.E. Purucker, R.A. Langel, M. Rajaram, C. Raymond, Global magnetization models with a priori information. J. Geophys. Res. **103**, 2563–2584 (1998)
M.E. Purucker, D. Ravat, H. Frey, C. Voorhies, T. Sabaka, M.H. Acuña, An altitude-normalized magnetic map of Mars and its interpretation. Geophys. Res. Lett. **27** (2000). doi:10.1029/2000GL000072
M.E. Purucker, B. Langlais, N. Olsen, G. Hulot, M. Mandea, The southern edge of cratonic North America: Evidence from new satellite magnetometer observations. Geophys. Res. Lett. **29** (2002). doi:10.1029/2001GL0136450
M.E. Purucker, T.J. Sabaka, S.C. Solomon, B.J. Anderson, H. Korth, M.T. Zuber, G.A. Neumann, Mercury's internal magnetic field: Constraints on large- and small-scale fields of crustal origin. Earth Planet. Sci. Lett. (2009). doi:10.1016/j.epsl.2008.12.017
Y. Quesnel, B. Langlais, C. Sotin, Local inversion of magnetic anomalies: Implication for Mars' crustal evolution. Planet. Space Sci. **55** (2007). doi:10.1016/j.pss.2006.02.004
Y. Quesnel, B. Langlais, C. Sotin, A. Galdéano, Modeling and inversion of local magnetic anomalies. J. Geophys. Eng. **5** (2008). doi:10.1088/1742-2132/5/4/003
Y. Quesnel, C. Sotin, B. Langlais, S. Costin, M. Mandea, M. Gottschalk, J. Dyment, Serpentinization of the martian crust during Noachian. Earth Planet. Sci. Lett. **277** (2009). doi:10.1016/j.epsl.2008.10.012
C.A. Raymond, J.L. Labrecque, Magnetization of the oceanic crust: thermoremanent magnetization or chemical remanent magnetization. J. Geophys. Res. **92**, 8077–8088 (1987)
R.D. Regan, J.C. Cain, W.M. Davis, Global magnetic anomaly map. J. Geophys. Res. **80**, 794–802 (1975)
C. Reigber, H. Lühr, S. P., CHAMP Mission Status. Adv. Space Res. **30** (2002). doi:10.1016/S0273-1177(02)00276-4
W.U. Reimold, R.L. Gibson, H. Henkel, Scientific comment on Muundjua et al., 2007: Magnetic imaging of the Vredefort impact crater, South Africa, EPSL 261, 456–468. Earth Planet. Sci. Lett. **273** (2008). doi:10.1016/j.epsl.2008.06.046
N.C. Richmond, L.L. Hood, A preliminary global map of the vector lunar crustal magnetic field based on Lunar Prospector magnetometer data. J. Geophys. Res. **113** (2008). doi:10.1029/2007JE002933
W. Riedler, K. Schwingenschuh, D. Moehlmann, V.N. Oraevskii, E. Eroshenko, J. Slavin, Magnetic fields near Mars – First results. Nature **341**, 604–607 (1989)
J.H. Roberts, R.J. Lillis, M. Manga, Giant impact on early Mars and the cessation of the Martian dynamo. J. Geophys. Res. **114** (2009). doi:10.1029/2008JE003287
P. Rochette, G. Fillion, R. Ballou, F. Brunet, B. Ouladdiaf, L.L. Hood, High pressure magnetic transition in pyrrhotite and impact demagnetization on Mars. Geophys. Res. Lett. **30** (2003). doi:10.1029/2003GL017359

S.K. Runcorn, On the interpretation of lunar magnetism. Phys. Earth Planet. Int. **10**, 327–335 (1975)
T.J. Sabaka, N. Olsen, M.E. Purucker, Extending comprehensive models of the Earth's magnetic field with Ørsted and CHAMP data. Geophys. J. Int. **159** (2004). doi:10.1111/j.1365-246X.2004.02421.x
J.A. Slavin, K. Schwingenschuh, W. Riedler, E. Eroshenko, The solar wind interaction with Mars – Mariner 4, Mars 2, Mars 3, Mars 5, and PHOBOS 2 observations of bow shock position and shape. J. Geophys. Res. **96**, 11235 (1991)
E.J. Smith, L.J. Davis, P.J. Coleman Jr., D.E. Jones, Magnetic field measurements near Mars. Science **149**, 1241–1242 (1965)
D. Smith, G. Neumann, R.E. Arvidson, E.A. Guinness, S.Slavney, Mars global surveyor laser altimeter mission experiment gridded data record. NASA Planetary Data System, MGS-M-MOLA-5-MEGDR-L3-V1.0 (2003)
S.C. Solomon, R.L. McNutt Jr., T.R. Watters, D.J. Lawrence, W.C. Feldman, J.W. Head, S.M. Krimigis, S.L. Murchie, R.J. Phillips, J.A. Slavin, M.T. Zuber, Return to Mercury: A global perspective on MESSENGER's first Mercury flyby. Science **321**, 59–62 (2008)
L.J. Srnka, Magnetic dipole moment of a spherical shell with TRM acquired in a field of internal origin. Phys. Earth Planet. Int. **11**, 184–190 (1976)
S. Stanley, J. Bloxham, W.E. Hutchison, M.T. Zuber, Thin shell dynamo models consistent with Mercury's weak observed magnetic field [rapid communication]. Earth Planet. Sci. Lett. **234** (2005). doi:10.1016/j.epsl.2005.02.040
A. Stephenson, Crustal remanence and the magnetic moment of Mercury. Earth Planet. Sci. Lett. **28**, 454–458 (1976)
D.J. Stevenson, Mercury's magnetic field – A thermoelectric dynamo? Earth Planet. Sci. Lett. **82**, 114–120 (1987)
D.J. Stevenson, Planetary magnetic fields. Earth Planet. Sci. Lett. **208** (2003). doi:10.1016/S0012-821X(02)01126-3
D.J. Stevenson, T. Spohn, G. Schubert, Magnetism and thermal evolution of terrestrial planets. Icarus **54**, 466–489 (1983)
F. Takahashi, M. Matsushima, Dipolar and non-dipolar dynamos in a thin shell geometry with implications for the magnetic field of Mercury. Geophys. Res. Lett. **33** (2006). doi:10.1029/2006GL025792
E. Thébault, A proposal for regional modelling at the Earth's surface, R-SCHA2D. Geophys. J. Int. **174** (2008). doi:10.1111/j.1365-246X.2008.03823.x
E. Thébault, L. Gaya-Piqué, Applied comparisons between SCHA and R-SCHA regional modeling techniques. Geochem., Geophys., Geosyst. **9** (2008). doi:10.1029/2008GC001953
E. Thébault, J.J. Schott, M. Mandea, Revised Spherical Cap Harmonic Analysis (R-SCHA): Validation and Properties. J. Geophys. Res. **111** (2006a). doi:10.1029/2005JB003836
E. Thébault, J.J. Schott, M. Mandea, Modeling the lithospheric magnetic field over France by means of revised spherical cap harmonic analysis (R-SCHA). J. Geophys. Res. **111** (2006b). doi:10.1029/2005JB004110
E. Thébault, K. Hemant, G. Hulot, N. Olsen, On the geographical distribution of induced time-varying crustal magnetic fields. Geophys. Res. Lett. **36** (2009). doi:10.1029/2008GL036416
J.M. Torta, L.R. Gaya-Piqué, A. De Santis, Spherical cap harmonic analysis of the geomagnetic field with application for aeronautical mapping, in *Geomagnetics for Aeronautical Safety: A Case Study in and Around the Balkans*, ed. by J.L. Rasson, T. Delipetrov (Springer, Dordrecht, 2006), pp. 291–307
S. Vennerstrom, N. Olsen, M.E. Purucker, M.H. Acuña, J.C. Cain, The magnetic field in the pile-up region at Mars, and its variation with the solar wind. Geophys. Res. Lett. **30** (2003). doi:10.1029:2003GL016883
F.J. Vine, D.H. Matthews, Magnetic anomalies over oceanic ridges. Nature **199**, 947–949 (1963)
Weiss et al., Space Sci. Rev. (2009, this issue)
P. Wessel, W.H.F. Smith, Free software helps map and display data. EOS, Trans. Am. Geophys. Union **72**, 441 (1991)
K.A. Whaler, R.A. Langel, Minimal crustal magnetization from satellite data. Phys. Earth Planet. Int. **48**, 303–319 (1996)
K.A. Whaler, M.E. Purucker, A spatially continuous magnetization model for Mars. J. Geophys. Res. **110** (2005). doi:10.1029/2004JE002393
J. Wicht, M. Mandea, F. Takahashi, U.R. Christensen, M. Matsushima, B. Langlais, The origin of Mercury's internal magnetic field. Space Sci. Rev. **132** (2007). doi:10.1007/s11214-007-9280-5